Available online at www.sciencedirect.com
ScienceDirect
Journal of Loss Prevention in the Process Industries 21 (2008) 162–184
Journal of Loss Prevention in the process industries
www.elsevier.com/locate/jlp

CFD modelling of hydrogen release, dispersion and combustion for automotive scenarios

A.G. Venetsanos[a,*], D. Baraldi[b], P. Adams[c], P.S. Heggem[d], H. Wilkening[b]

[a]*National Centre for Scientific Research Demokritos, Environmental Research Laboratory, Institute of Nuclear Technology and Radiation Protection, 15310 Aghia Paraskevi, Attiki, Greece*
[b]*Joint Research Centre European Commission, Nuclear Safety Unit, Westerduingweg 3, P. Box 2, 1755 ZG Petten, Netherlands*
[c]*Volvo Technology Corp. Department, 06120 Chalmers Teknikpark, 412 88 Gothenberg, Sweden*
[d]*Raufoss Fuel System AS, N-2831 Raufoss, Norway*

Received 19 April 2007; received in revised form 15 June 2007; accepted 15 June 2007

Abstract

The paper describes the analysis of the potential effects of releases from compressed gaseous hydrogen systems on commercial vehicles in urban and tunnel environments using computational fluid dynamics (CFD). Comparative releases from compressed natural gas systems are also included in the analysis.

This study is restricted to typical non-articulated single deck city buses. Hydrogen releases are considered from storage systems with nominal working pressures of 20, 35 and 70 MPa, and a comparative natural gas release (20 MPa). The cases investigated are based on the assumptions that either fire causes a release via a thermally activated pressure relief device(s) (PRD) and that the released gas vents without immediately igniting, or that a PRD fails. Various release strategies were taken into account. For each configuration some worst-case scenarios are considered.

By far the most critical case investigated in the urban environment, is a rapid release of the entire hydrogen or natural gas storage system such as the simultaneous opening of all PRDs. If ignition occurs, the effects could be expected to be similar to the 1983 Stockholm hydrogen accident [Venetsanos, A. G., Huld, T., Adams, P., & Bartzis, J. G. (2003). Source, dispersion and combustion modelling of an accidental release of hydrogen in an urban environment. *Journal of Hazardous Materials*, *A105*, 1–25]. In the cases where the hydrogen release is restricted, for example, by venting through a single PRD, the effects are relatively minor and localised close to the area of the flammable cloud. With increasing hydrogen storage pressure, the maximum energy available in a flammable cloud after a release increases, as do the predicted overpressures resulting from combustion. Even in the relatively confined environment considered, the effects on the combustion regime are closer to what would be expected in a more open environment, i.e. a slow deflagration should be expected.

Among the cases studied the most severe one was a rapid release of the entire hydrogen (40 kg) or natural gas (168 kg) storage system within the confines of a tunnel. In this case there was minimal difference between a release from a 20 MPa natural gas system or a 20 MPa hydrogen system, however, a similar release from a 35 MPa hydrogen system was significantly more severe and particularly in terms of predicted overpressures. The present study has also highlighted that the ignition point significantly affects the combustion regime in confined environments. The results have indicated that critical cases in tunnels may tend towards a fast deflagration, or where there are turbulence generating features, e.g. multiple obstacles, there is the possibility that the combustion regime could progress to a detonation.

When comparing the urban and tunnel environments, a similar release of hydrogen is significantly more severe in a tunnel, and the energy available in the flammable cloud is greater and remains for a longer period in tunnels. When comparing hydrogen and natural gas releases, for the cases and environments investigated and within the limits of the assumptions, it appears that hydrogen requires different mitigation measures in order that the potential effects are similar to those of natural gas in case of an accident. With respect to a PRD

*Corresponding author. Tel.: +30 210 6503402; fax: +30 210 6525004.
E-mail addresses: venets@ipta.demokritos.gr (A.G. Venetsanos), daniele.baraldi@jrc.nl (D. Baraldi), paul.adams@volvo.com (P. Adams), psh@rafs.no (P.S. Heggem), heinz.wilkening@jrc.nl (H. Wilkening).

0950-4230/$ - see front matter
doi:10.1016/j.jlp.2007.06.016

opening strategy, hydrogen storage systems should be designed to avoid simultaneous opening of all PRD, and that for the consequences of the released energy to be mitigated, either the number of PRDs opening should be limited or their vents to atmosphere should be restricted (the latter point would require validation by a comprehensive risk assessment).

Keywords: Combustion; Dispersion; Hydrogen safety; Release; Urban environment; Tunnel environment

1. Introduction

Hydrogen is currently regarded as a promising energy carrier for the future with many potential applications. Hydrogen offers the prospect of solutions to issues such as reduction of air pollution, security of energy supply, and climate change, especially when produced with renewable energy sources. Hydrogen provides the possibility of sustainable transportation in the future, and it is estimated that a transition to hydrogen as the main automotive energy carrier could be completed by the middle of this century (HLG, 2003; US Department of Energy, 2002). In this context, hydrogen safety is one of the key enabling factors in the move towards a hydrogen economy. In particular, the safety of hydrogen storage systems in automotive and other applications is one of the crucial technological issues to be addressed. On-board hydrogen storage is another key enabling factor due to the low density of hydrogen. In automotive applications, compressed gas storage systems at 20–70 MPa or liquid cryogenic storage systems at −253 °C are the only current technologies that are capable of providing an acceptable balance of vehicle range, storage volume and weight, and system costs.

A risk analysis is a primary element in assessing the safety of a new technology, and one of the essential stages of a risk analysis is the evaluation of event consequences. In the context of safety, risk can be defined as the combination of the probability of occurrence of harm and the severity of that harm (ISO-IEC Guide 51, 1999). In the paper only the later aspect of the risk definition is investigated. A key component of a risk analysis of fuel storage systems is developing an understanding of the behaviour of fuel releases in realistic scenarios, whether they are unintentional or intentional. Such knowledge allows the development of measures to minimize the probability of an accident, and of methods to mitigate the consequences if an accident should occur.

Since it is quite expensive to undertake experimental hydrogen release and combustion in real-scale configurations, the use of computational fluid dynamics (CFD) modelling for safety purposes is increasing in this field. Moreover CFD modelling also permits the investigation of releases in real world environments. Earlier hydrogen safety work in urban environment based on CFD methods of investigation includes the analysis of the 1983 Stockholm accident by Venetsanos, Huld, Adams, and Bartzis (2003). To the author's knowledge, the present work is the first safety study of hydrogen commercial vehicles in urban environments based on the CFD methodology. In the Stockholm accident, a hydrogen leak occurred from a rack of hydrogen cylinders located on a truck delivering industrial gases. In the subsequent explosion in an inner city area, several people were injured, the façade of the nearest building was heavily damaged and windows were broken within a radius of 90 m.

Regarding the tunnel environment, previous safety studies with CFD methodology include the work that was undertaken within the EIHP Phase 1 (Adams, 2000) on the release of liquid and compressed gaseous hydrogen from vehicles in tunnels (Wilkening, Venetsanos, Huld, & Bartzis, 2000). Similar work was performed by FZK (1999). The CFD approach has also been used earlier by Zalosh, Amy, Hofmeister, and Wang (1994) to evaluate the consequences of natural gas releases from compressed natural gas (CNG) vehicles in tunnels. Fire safety research activities in tunnels reported by Rhodes (2003) should also be mentioned, even if not directly related to hydrogen safety. CFD simulations of gaseous explosions from high pressure releases from natural gas pipes in tunnels have been reported by Niederbäumer, Sägesser, and Obrist (2004). CFD simulation of hydrogen dispersion in tunnels was recently reported by Mukai, Suzuki, Mitsuishi, Oyakawa, and Watanabe (2005). The amount of hydrogen leaked was 60 m^3 (approximately 5.08 kg), which corresponds to the amount necessary for future fuel cell vehicles to achieve their desired running distance. The evaluation of risk for hydrogen releases in tunnels from private and commercial vehicles is the subject of current research work within the HyTunnel activity of the HySafe Network of Excellence (www.hysafe.org), funded by the EC. Applications of the CFD approach for hydrogen releases in confined spaces (other than tunnels) was performed by Breitung, Necker, Kaup, and Veser (2001) for a private garage and by Swain and Swain (1992) for releases in a confined environment such as a kitchen.

The present study was based on commercial vehicles as they may store on-board a quantity of hydrogen, typically an order of magnitude larger than many passenger cars. The scope of this paper is restricted to typical city buses, i.e. standard urban public buses. Hydrogen releases from storage systems with nominal working pressures between 20 and 70 MPa are considered, along with a comparative natural gas release from a 20 MPa system. High pressure gaseous fuel storage systems for automotive applications are equipped with temperature triggered pressure relief devices (PRD) that open and release the gas to the external environment in order to limit a potentially dangerous internal pressure increase in the event of a fire. Three different release strategies are investigated.

Worst case scenarios in which a chain of events occurs at critical moments (i.e. low probability events) have been investigated. For example, the maximum quantity of fuel is assumed to be on-board before the release. Once the worst cases are understood, preventive and mitigating measures can be developed. Event sequences with higher probabilities of occurrence and reduced consequences were not considered as part of this initial study.

The goals of the work described in this paper are to:

- predict and understand the dispersion and combustion of hydrogen and natural gas in realistic release scenarios;
- assist development of safe compressed gas hydrogen (CGH2) components and systems;
- provide input to the continuing development of legal requirements for automotive CGH2 systems; and
- provide an informed basis for discussion with the authorities and public regarding the introduction of hydrogen as an automotive fuel.

The work in this paper was undertaken as part of a broader investigation that was carried out within the European Integrated Hydrogen Project—Phase 2 (EIHP-2) (www.eihp.org) of the European Commission's 5th Framework Research Programme.

2. Methodology

The methodology adopted is similar to that used in the earlier Stockholm accident study (Venetsanos et al., 2003). It is based on five main stages:

- Identification of release scenarios;
- Release source calculations;
- Dispersion calculations;
- Combustion calculations; and
- Analysis of results.

The release calculations provide the release boundary conditions necessary for the subsequent dispersion calculations. The dispersion calculations provide the gas distribution that is used as the initial condition for the combustion calculations. The release, dispersion and combustion calculations have been performed using the same codes and models that were employed in the Stockholm accident analysis (Venetsanos et al., 2003). More specifically the ADREA-HF code (Bartzis, 1991; Würtz et al., 1996) was applied for dispersion and the REACFLOW code (Wilkening & Huld, 1999) for combustion.

3. Scenarios

3.1. Fuels

As discussed in Section 1, hydrogen is seen as a fuel with significant future potential for automotive applications, and it forms the basis of the study. It is also important to understand the safety-related behaviour of fuels in comparison with each other, and particularly where the fuels are stored in a similar manner such as compressed gas, e.g. CGH2 and CNG. A cursory inspection would indicate that CGH2 and CNG systems should be similar as they both store flammable gas at high pressure. However, the different behaviour of the gases, when released from the systems, either unintentionally, e.g. as a result of an accident, or intentionally, e.g. via operation of a PRD, requires further investigation in order to assess whether the design of the components or systems have to be reconsidered.

3.2. Vehicle

Commercial vehicles are of particular interest in fuel-related safety studies since they have a fuel capacity much larger than that of passenger cars by up to an order of magnitude. To achieve a realistic operating range, a typical passenger car would require approximately 4 kg of hydrogen assuming a fuel cell drive-train, while a typical city bus would require up to approximately 40 kg of hydrogen. City buses are usually refilled at a central location, which is one of the factors enabling them to be an early application of hydrogen. For these reasons, urban or city buses have been chosen as the basis of this study.

A typical non-articulated single deck city bus is assumed as the basis of the study. Typical dimensions assumed for the bus are: length 12 m, width 2.55 m, and a height of approximately 3 m.

3.3. On-board storage system

There are many possible configurations of on-board CGH2/CNG storage systems for city buses. Consequently, a configuration representative of typical European practice has been selected. The fuel storage system is placed on the roof of the bus and forward of the mid-point, as shown in Fig. 1.

The notional storage system comprised 2 bundles of 4 cylinders each, i.e. 8 cylinders in total, as shown in Fig. 2. The system follows the requirements of the draft UN ECE regulation for CGH2 vehicle components and systems (UN ECE WP29 GRPE, 2004) with temperature triggered PRD in both ends of each cylinder and with an automatic valve securing the fuel supply line from each cylinder. A notional arrangement has been selected for the PRD vents where groups of four PRD vents are mainfolded into four main vents. These outlet pipes have been assumed to be routed above the cylinders and point vertically upwards from the roof of the bus.

Forty kilograms of hydrogen was selected as being representative of the typical maximum quantity that a fuel cell powered city bus would carry in order to achieve an operating range of up to approximately 400 km (Adams et al., 2004). One hundred and sixty eight kilograms of

natural gas have been selected as being representative of a typical CNG city bus (Heggem, 2002).

The nominal working pressure of the CNG system was taken as 20 MPa in line with current practice. For the CGH2 scenarios, 3 nominal working pressures have been considered: 20, 35 and 70 MPa. For CGH2 systems the lower pressure is likely to be 25 MPa based on current industry trends. However, a pressure of 20 MPa has been chosen, as this would provide a direct comparison between hydrogen and natural gas systems at the same pressure. Based on a recent study, it seems likely that CGH2 systems for city buses do not need to use systems with pressures in excess of 35 MPa (Adams et al., 2004).

Fig. 1. Typical city bus with roof mounted gaseous fuel storage system.

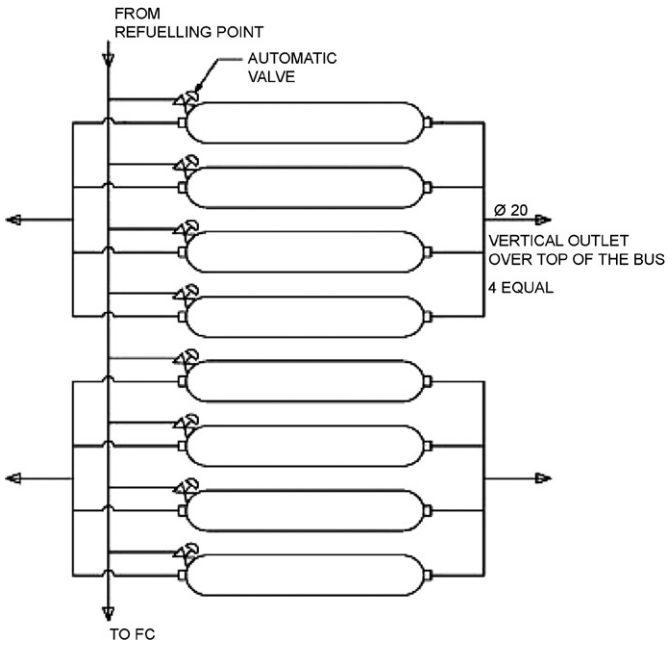

Fig. 2. Assumed storage system arrangement.

Different storage volumes are required for the different fuels, quantities and nominal working pressures. The different storage volume has been achieved by varying the length of the cylinders and keeping their diameter constant. Other than that, the fuel system and vent line geometry have been assumed to be the same for the different gases and storage pressures. Table 1 describes the principle storage system volumes and stored fuel masses for the various configurations.

3.4. Possible fuel release scenarios

The possible fuel release scenarios are based on the assumption that either fire causes a release via a thermally activated PRD and that the released gas vents without immediately igniting, or that a PRD fails. Among the several possible PRD release configurations, three have been identified as the most representative, including a worst-case scenario. The scenarios are illustrated in Table 2. In Case 1, only one PRD is assumed to be open and all automatic valves are closed, therefore the contents of only one cylinder is released through one vertical outlet above the roof. Case 2 differs from Case 1 in that all automatic valves are open and therefore the gas from all cylinders is released into the atmosphere through one vertical outlet. In Case 3 (worst case scenario), all PRDs and automatic valves are open and the gas from all cylinders is released through the four vertical outlets over the roof. In Table 2, the selected scenarios are described. Case 3 is an upper bound scenario as all PRDs are unlikely to trigger at the same moment. A more likely scenario would be that a large fire causes the PRDs to open independently of each other. However, as there are many possible permutations for such a scenario depending on the bus, the storage system and the fire, it was considered more important to understand the outer envelope of possible releases.

4. Mathematical formulation

4.1. Release source term

The source system (storage system) was modelled, by assuming *Fanno* flow in the pipes and isentropic change in the tanks, using real hydrogen properties (AL, 1976).

Table 1
Storage system details

Fuel	Pressure (MPa)	Fuel density at 15 °C (kg m^{-3})	Total storage volume (l)	Single cylinder volume (l)	Total fuel mass (in 8 cylinders) (kg)	Fuel mass in one cylinder (kg)
H_2	20	14.96	2672	334	40	5
H_2	35	24.02	1600	200	40	5
H_2	70	40.18	996	124.5	40	5
CH_4	20	168	1000	125	168	21

Table 2
Fuel release scenarios selected for the modelling

Case no.	Possible release	Description	Gas released (kg)
1	Vehicle out of service (automatic valves closed) and one random PRD fuse fails open OR Fire causes a single PRD to trigger[a]	Gas from one cylinder released through 1 PRD vent and 1 outlet	Hydrogen—5 Natural gas—21
2	Vehicle in service (automatic valves open) and one random PRD fuse fails open OR Fire causes a single PRD to trigger[a]	Gas from all cylinders released through 1 outlet	Hydrogen—40 Natural gas—168
3	Fire causes all PRDs to trigger simultaneously[a]	Gas from all cylinders released through all 4 outlets	Hydrogen—40 Natural gas—168

[a]It is assumed that the fire does not ignite the gas. Anecdotal reports by various research and testing organizations indicate that fires that cause temperature triggered PRD to open may not immediately ignite the vented gas. The fire that triggers the thermally activated PRD may not be in a position that causes the vented gas to ignite, since the exit from the vent may not be situated in the fire.

The relevant model equations are given below (see also John, 1978; Rogers & Mayhew, 1992).

Pipe mass, energy and momentum conservation:

$$\mathrm{d}(\rho u)=0,\ \ \mathrm{d}h+u\mathrm{d}u=0,\ \ \rho u\,\mathrm{d}u+\mathrm{d}P+\frac{\lambda}{2}\rho u^2\frac{\mathrm{d}x}{D}=0. \tag{1}$$

Tank j mass and energy conservation:

$$\frac{\mathrm{d}V_j\rho_j}{\mathrm{d}t}=\sum_i F_{ij},\ \ i=0,\ N_{pj},\ \ \gamma\frac{\mathrm{d}\rho_j}{\rho_j}=\kappa\,\mathrm{d}P_j, \tag{2}$$

where N_{pj} is the number of pipes connected to the tank j and F_{ij} the mass flow rate in pipe i, connected to tank j, positive if the flow is into the tank, V_j is the tank j volume, u is the pipe velocity, D the pipe diameter, x the distance from pipe entrance, t the time, P is the pressure, λ is the resistance coefficient (smooth pipes were assumed), $\gamma=c_p/c_V=1.4$ In the above equations enthalpy h and density ρ were obtained from the following non-ideal gas relations:

Enthalpy as function of temperature and pressure:

$$\mathrm{d}h=c_P\,\mathrm{d}T+(1-\beta T)\frac{\mathrm{d}P}{\rho}, \tag{3}$$

Compressibility coefficients:

$$\beta=\frac{1}{T}+\frac{1}{z}\left(\frac{\partial z}{\partial T}\right)_P,\ \ \kappa=\frac{1}{P}-\frac{1}{z}\left(\frac{\partial z}{\partial P}\right)_T. \tag{4}$$

Equation of state:

$$z=z(T,P)\equiv\frac{P}{\rho RT}. \tag{5}$$

The numerical procedure of solving Eqs. (1)–(5) above consists of two major steps. For given tank conditions at a given time (t) the mass flow rate through the pipes is first calculated by solving Eq. (1), making also use of relations (3)–(5). Then using the obtained pipe flow rates, new tank conditions are calculated at the new time ($t+\mathrm{d}t$) from Eq. (2) and the procedure is repeated from step 1, until mass flow rates become zero.

The above model does not account for heat transfer from ambient air to the hydrogen through the tank and pipes' walls. Recent experiments and simulations performed by Schefer, Houf, Williams, Bourne, and Colton (2006) have shown that heat trasfer through the walls affects release conditions and that this effect although small at the beginning increases with time. In the present work, the effect of non-accounting for such heat trasfer mechanisms is considered to be small, given that ignition was assumed at the time of maximum flammable hydrogen mass, which generally occurs at the early stages of the release, that is when the departure from the adiabatic release conditions is not large.

4.2. Dispersion and combustion

The present formulation uses the CFD approach for both the dispersion and combustion calculations. The dispersion and combustion models solve the conservation equations for mass, chemical species, momentum and energy. This set of conservation equations can be written in general integral form (Grasso & Meola, 1996).

$$\frac{\partial}{\partial t}\left(\int_\Omega U\,\mathrm{d}V\right)+\int_{S\Omega}n_iF_{i,conv}\,\mathrm{d}A=\int_{S\Omega}n_iF_{i,diff}\,\mathrm{d}A+\int_\Omega S\,\mathrm{d}V, \tag{6}$$

where $U=(\rho_\gamma,\rho u_j,\rho E,\rho h)^{\mathrm{T}}$ is the vector of conserved quantities which are the unknowns of the system. Here, $\rho_\gamma,(\gamma=1,\Gamma)$ are the partial densities, ρu_j is the momentum vector, ρE is the total energy (used only in REACFLOW) and ρh the enthalpy (used only in ADREA-HF). The other terms are given as follows:

Convective fluxes:

$$F_{i,conv}=\left(\rho_\gamma u_i,\rho u_iu_j+p\delta_{ij},\rho u_i\left(h+\frac{u_i^2}{2}\right),\rho u_ih\right)^{\mathrm{T}}. \tag{7}$$

Diffusive fluxes:

$$F_{i,diff} = \begin{pmatrix} D_\gamma \frac{\partial Y_\gamma}{\partial x_i}, \tau_{ij}, \sum_{\gamma=1}^{\Gamma} h_\gamma D_\gamma \frac{\partial Y_\gamma}{\partial x_i} + \lambda \frac{\partial T}{\partial x_i} + \tau_{ij} u_j \\ , \sum_{\gamma=1}^{\Gamma} h_\gamma D_\gamma \frac{\partial Y_\gamma}{\partial x_i} + \lambda \frac{\partial T}{\partial x_i} \end{pmatrix}^T. \quad (8)$$

Source terms (including chemical reactions, for REACFLOW only):

$$S = \left(-\dot{\rho}_\gamma, -\rho g_j, -\rho g_j u_j - \sum_{\gamma=1}^{\Gamma} \dot{\rho}_\gamma \Delta h_\gamma^f, \frac{Dp}{Dt} \right)^T, \quad (9)$$

where h_γ, $Y_\gamma, (\gamma = 1, \Gamma)$ are the partial enthalpies and mass fractions, $\dot{\rho}_\gamma$, the chemical production rates, Δh_γ^f the formation enthalpies, g_j the acceleration of gravity, T the temperature, τ_{ij} the shear stress tensor, D_γ the scalar transport diffusivities and λ the effective conductivity.

Closure of this system of equations is done with an equation of state, which for both the dispersion and the combustion codes is a variant on the equation for an ideal mixture of gases. Real hydrogen compressibility factors were used in the dispersion code. Temperature dependent mixture components heat capacities were used in both codes.

In both codes turbulence is modelled using the eddy viscosity formulation.

In the dispersion code it is simulated using a non-isotropic one-equation turbulence model, which solves the turbulent kinetic energy conservation equation, employs analytic formulas to derive the length scales, which depend on distance from nearest solid, on stability and on global acceleration parameter and obtains the dissipation rate of turbulent kinetic energy as function of turbulent kinetic energy and the length scales, see Statharas, Venetsanos, Bartzis, Würtz, and Schmidtchen (2000) for details.

The combustion model employs a compressible version of the classical two-equation k–ε equations. The turbulent quantities serve to calculate the turbulent viscosity for the Favre-averaged flow equations (Wilkening & Huld, 1999). At the same time the turbulent quantities are employed as input for a model for the turbulent combustion. The model employed is based on the eddy–dissipation model developed by Hjertager (1982a, b, 1989). The model has been extensively validated by Hjertager and his co-workers in Hjertager (1993), Hjertager and Solberg (1999) and Popat et al. (1996).

The expression of the chemical reaction rate for turbulent combustion is given by the expression of the rate of change of the fuel partial density

$$\dot{\rho}_{fuel} = -c_{fo} \left(1 + \frac{4.4}{1 + 3.2(\sqrt{k}/S_{lam})} \right) \frac{\varepsilon}{k} \rho Y_{lim} \quad \text{if } \tau_{ch}/\tau_{tu} \langle D_{ie}$$

$$\dot{\rho}_{fuel} = 0 \quad \text{if } \tau_{ch}/\tau_{tu} \geqslant D_{ie} \quad (10)$$

where $\dot{\rho}_{fuel}$ is the mean fuel consumption rate (expressed in term of the fuel partial density), Y_{lim} is the mass fraction of the chemical species which is present in least concentration, stoichiometrically weighted, ρ is the density, D_{ie} is a constant, typically $D_{ie} = 1000$, and k and ε are the turbulent kinetic energy and the dissipation rate of turbulent kinetic energy, respectively. The turbulent time scale τ_{tu} and the chemical time scale τ_{ch} are described by the expressions

$$\begin{cases} \tau_{ch} = A_{ch} T^{B_{ch}} e^{-E_{ch}/RT}, \\ \tau_u = k/\varepsilon, \end{cases} \quad (11)$$

D_{ie}, c_{f0}, A_{ch}, B_{ch} and E_{ch} being empirical constants that have been taken from Hjertager (1982b). The laminar flame speed S_{lam} depends on the local hydrogen concentration. In the calculations it has been assumed to vary in a polynomial fashion, with a polynomial fitted from published data (Koroll, Kumar, & Bowles, 1993).

REACFLOW employs a finite-volume scheme on an unstructured 3-D computational mesh. The mesh is composed of tetrahedral cells and the geometrical treatment is very similar to the one proposed by Nkonga and Guillard (1994). Variants of Roe's (1980) approximate Riemann solver have been implemented in the code. The geometric flexibility of an unstructured tetrahedral computational mesh is combined with adaptive meshing in space and time to provide high computational efficiency. By means of the adaptive meshing, a fine resolution is used only where is required, e.g. the flame front while in other regions of the flow a significantly lower resolution can be employed without loss of accuracy (Naamansen, Baraldi, Hjertager, Solberg, & Cant, 2002). The 3D version of adaptive meshing (Troyer, Baraldi, Kranzlmueller, Wilkening, & Volkert, 2005) is very similar to that of Rivara and Levin (1992).

Validation studies have been performed with REACFLOW by mean of comparisons between simulation results and experimental data. Some of the validation studies have been published, see Huld, Peter, and Staedtke (1996), Wilkening and Huld (1999), Bielert et al. (2001, 2003), Baraldi et al. (2003), Gallego et al. (2005), Breitung et al. (2005), Wilkening and Baraldi (2006).

For ADREA-HF code validation studies, the reader can refer to Statharas, Bartzis, Venetsanos, and Würtz (1993), Andronopoulos, Bartzis, Würtz, and Asimakopoulos (1994), Würtz et al. (1996), Venetsanos, Bartzis, Würtz and Papailiou (2000), Statharas et al. (2000), Vlachogiannis, Rafailidis, Bartzis, Andronopoulos, and Venetsanos (2002), Gallego et al. (2007), Venetsanos and Bartzis (2007).

5. Urban environment

5.1. Modelling strategy

The scenario was based on a city bus located in the same environment, where the 1983 Stockholm accident occurred (Venetsanos et al., 2003). It is an urban environment in

central Stockholm, typical of urban residential areas in many European cities, where streets are enclosed by relatively tall buildings. The bus location and building dimensions are provided in Figs. 3 and 4. Typical meteorological conditions for Stockholm have been assumed based on data collected for the modelling of the 1983 Stockholm accident: 3.88 m/s average wind speed at 10 m height, 270° prevailing meteorological wind direction (West wind) and average air temperature −1.4 °C. The angle between wind direction and X axis is 20°, see Fig. 4.

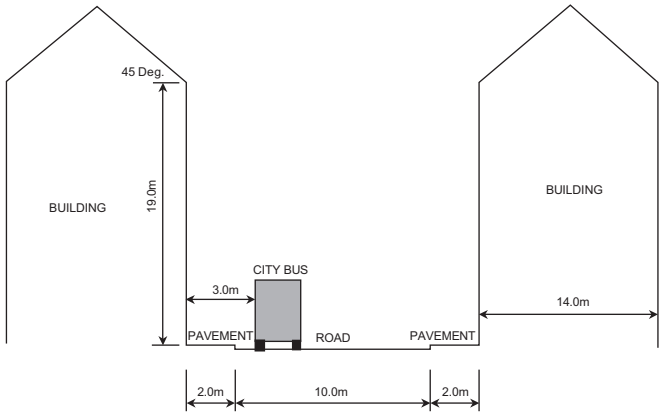

Fig. 3. Urban environment—dimensions.

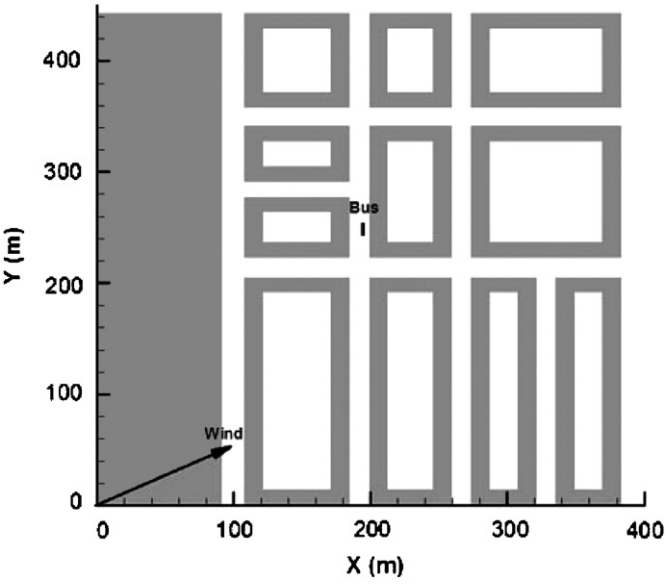

Fig. 4. Urban environment—bus location and wind direction (top view).

Table 3 shows the fuel release scenarios that have been modelled.

5.1.1. Release

The source model developed for the Stockholm accident (Venetsanos et al., 2003) has been applied to obtain the release exit conditions as a function of time. The source model has been based on the real-gas properties of hydrogen. Natural gas is a mixture of gases with varying composition, depending on its natural source. In the modelling, the real physical properties of methane have been assumed for natural gas, since natural gas is composed mainly by methane by molar volume.

5.1.2. Dispersion

The domain dimensions were 380 × 440 × 180 m in the X, Y and Z directions, respectively. The buildings were assumed to be six stories high with inclined 45° roofs and internal courtyards. From aerial photos it was estimated that the buildings are approximately 14 m wide. The grid is Cartesian, non-equidistant comprised of 60 × 58 × 41 cells. The minimum horizontal cell dimension was 1.4 m in the region of the bus. The minimum vertical cell dimension was 0.5 m close to ground. The grid expansion ratio was 1.12.

The four storage system outlets were modelled as four vertical jet area sources located vertically immediately above the roof of the bus and horizontally at distances 2.25 (for outlets 2 and 4) and 3.75 m (for outlets 1 and 3) from the front of the bus and 0.7 m from the lateral sides of the bus. For Case 3, all four jet area sources were activated, while for Cases 1 and 2 only the source corresponding to outlet 1 was activated. It should be noted that the present area source approach preserves release mass, momentum and energy flow rates and the area sources do not coincide with computational cell faces but are rather treated as source terms in the mass, momentum and energy equations.

Table 3
Modelled fuel release scenarios (urban environment)

Fuel/pressure (MPa)	Case 1		Case 2		Case 3	
	Dispersion model	Combustion model	Dispersion model	Combustion model	Dispersion model	Combustion model
Hydrogen						
20	*Y*	–[a]	*Y*	*Y*	*Y*	*Y*
35	*Y*	*Y*	*Y*	*Y*	*Y*	*Y*
70	*Y*	*Y*	–[c]	–[c]	*Y*	*Y*[b]
Natural gas						
20	*Y*	–[a]	*Y*	–[a]	*Y*	*Y*

[a]Flammable mass is too small to generate significant overpressures.
[b]Effects of changing the position of the ignition point were investigated.
[c]Case 2 for hydrogen stored at 70 MPa was not modelled as the results could be estimated from Cases 1 and 3, and the other Case 2 results.

The horizontal cell size close to the source(s) is by factor of 2–5 higher than what one would get using Birch type equivalent source diameter approaches, Birch, Brown, Dodson, and Swaffield (1984), Ewan and Moodie (1986) and Birch, Hughes, and Swaffield (1987). The present choice was a compromise made in order to limit the total number of computational cells, having in mind that mass, momentum and energy source release rates are not affected by grid size, since the jet area sources used did not coincide with computational cell faces, as already mentioned above.

Dispersion calculations have been performed in three phases. At first the steady state vertical profiles of the approaching wind were calculated. In the second phase the calculated 1-*d* profiles were used as initial condition to calculate the 3-*d* steady state wind field over the entire site. In the third phase the 3-*d* steady state wind field from the second phase was used as the initial condition for the subsequent 3-*d* transient dispersion calculation.

Boundary conditions for the 3-*d* calculations were as follows. Standard log-layer wall functions for velocity and turbulent kinetic energy were used on solid surfaces (see also Venetsanos and Bartzis, 2007). A roughness of 0.001 m was assumed for the bus and buildings and 0.1 m for the ground. Dirichlet (given value) plus Neumann (zero gradient) boundary conditions were used for the inflow domain lateral planes and the source(s). Neumann boundary conditions were used at the top of domain, except for the *w*-velocity, for which a zero value was assumed. Neumann boundary conditions were used for the outflow domain lateral planes.

5.1.3. Combustion

CFD combustion calculations were performed using the REACFLOW code (Troyer et al., 2005; Wilkening & Huld, 1999). The hydrogen distribution and the flow conditions (velocity, temperature, pressure, turbulent kinetic energy and dissipation rate of turbulent kinetic energy) at the time of the maximum flammable fuel mass were used as initial conditions for the combustion calculations.

The computational domain for the combustion calculations has the dimensions of $182 \times 202 \times 50$ m. The grid is unstructured and it consists of tetrahedral cells. The initial number of computational nodes (cells) is about 40,000 (206,000). The minimum grid size close to the bus region is about 0.3 m rising to >3 m at the corners of the domain. In Venetsanos et al. (2003), two grids were employed for the combustion calculations because the initial explosion was located among the gas bottles on the delivery truck. This ignition configuration required an initial fine mesh in the ignition region because of geometrical details. In this paper, being the ignition on the top of the bus, the requirements for such a fine mesh in the ignition region do not hold. Therefore the combustion calculations were performed only on a computational mesh similar to the second grid used in Venetsanos et al. (2003). Adaptive meshing (Troyer et al., 2005; Wilkening & Huld, 1999; Wilkening & Baraldi, 2006) was employed with $\Delta x \approx 0.1$ m, bringing the initial number of nodes from 40,000 up to 400,000, during the calculations, depending on the case. Grid adaptation was based on the temperature difference between two grid-points, which is usually large within the flame front. Due to the nature of the adaptation algorithm adaptation occurs already a few grid cells ahead of the flame (Wilkening & Huld, 1999). In order to avoid the issue of grid dependency, it must be emphasized that for the mesh resolution, the same values or very close value to the mesh resolution in the validation calculations were selected.

5.2. Results and discussion

5.2.1. Release

The predicted mass flow rates for Cases 1, 2 and 3 are shown in Figs 5–7, respectively. A diameter of 6 mm was assumed for each PRD line. The mass flow rates shown for Case 3 are the sum from all four outlets. Calculated flow rates depend on the physical properties of the fuel, on the initial storage pressure, on the amount of mass stored and on the exit cross-section.

For a given fuel release scenario, an increase in initial storage pressure leads to higher mass flow rates and shorter system emptying times. For a given initial storage pressure and exit cross-section the mass flow rates are initially the same, independent of the amount of mass stored. This can be observed by comparing Cases 1 and 2 for times close to the start of release. As the release proceeds, the mass flow rate for Case 2 decreases more slowly than for Case 1. For methane, mass flow rates are larger than for hydrogen. The higher density of methane and the larger initial amount of methane in the tank cause a larger and longer lasting mass flow rate for methane than for hydrogen.

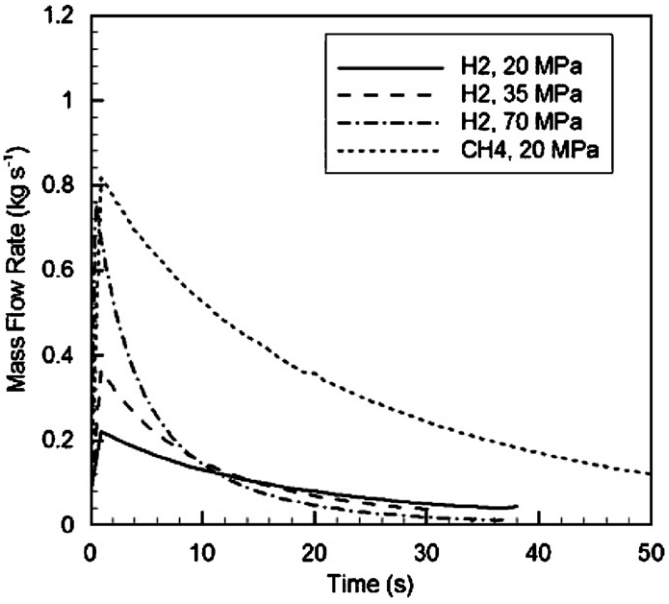

Fig. 5. Mass flow rate history for Case 1.

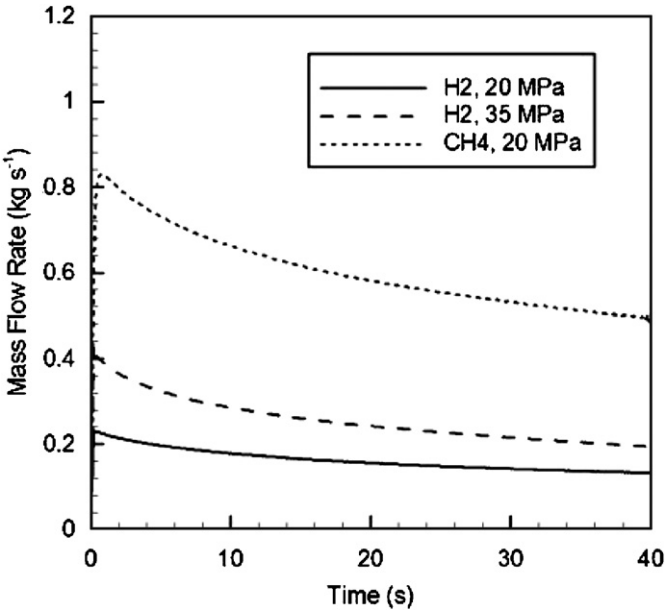

Fig. 6. Mass flow rate history for Case 2.

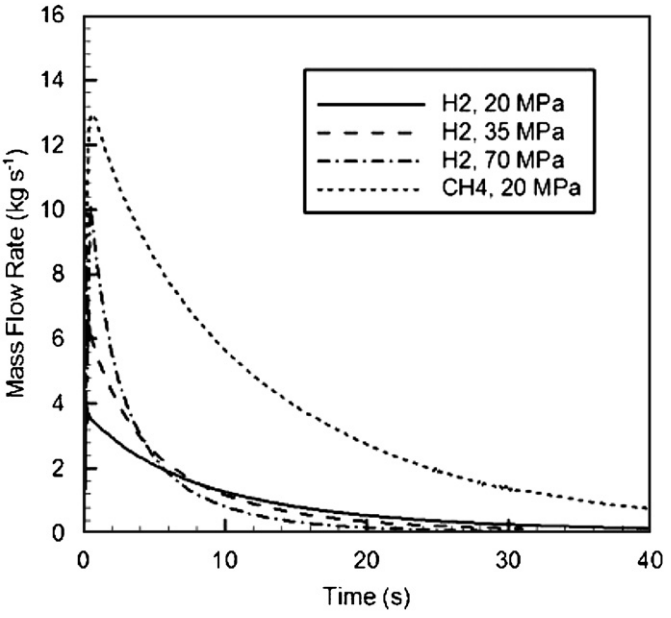

Fig. 7. Mass flow rate history for Case 3.

5.2.2. Dispersion

The flammable masses of fuel at a given time after the start of the release are illustrated in Figs. 8–10 (left hand side) for Cases 1, 2 and 3, respectively. The flammable masses refer to the mass of fuel between the appropriate lower and upper flammability limits. As expected, the predicted values indicate that Case 3 (rapid release of all fuel) leads to the largest flammable masses and Case 1 (release of fuel from only one cylinder through one outlet) to the lowest. From the shapes of the predicted curves it can be observed that peaks occur relatively soon after the start of release. The presence of these peaks is a result of the release mass flow rate decreasing with time. The level and time of occurrence of these peaks depends on initial storage pressure. For a given scenario, an increase in initial storage pressure leads to higher peaks at shorter times after the start of the release.

For methane the predicted flammable masses are comparable to hydrogen for Case 3 but are significantly smaller in the other two cases. This behaviour was unexpected given the larger methane mass flow rates in all cases, as mentioned earlier. The behaviour for Cases 1 and 2 can be attributed to the wider flammability range of hydrogen (0.04–0.75 by vol. concentration) compared to methane (0.053–0.15) and to its higher tendency to expand and occupy larger volumes than methane leading to higher concentrations. The behaviour for Case 3 can be attributed to the higher mass flow rate of methane and to less intense turbulent mixing. The last factor is a result of the lower sonic velocities at the jet source exit and of the lower buoyancy of methane compared to hydrogen.

The predicted hydrogen (35 MPa) and methane (20 MPa) lower flammability limit (LFL) clouds at the time of the maximum predicted flammable fuel mass are shown in Figs. 11 and 12 for Cases 1 and 3, respectively. For Case 3 the LFL clouds exceed the height to the start of the inclined roofs. Consequently streetlights, electrical signs, air-conditioning units, etc. may well fall within the LFL cloud and serve as potential ignition sources. Hydrogen LFL clouds are more flattened near their top than methane, showing a tendency for horizontal dispersion. In general, the predicted LFL clouds are skewed with respect to the vertical direction. This is a result of the assumed ambient wind conditions.

The theoretical chemical energy present as a function of time has been evaluated in the analysis. The energy has been estimated by multiplying the mass of fuel by the lower heat of combustion per unit weight; see Table 4. The theoretical energy history of the released fuel within flammable concentrations is shown on the right hand side of Figs. 8–10. The energy peaks occur soon after the start of the release for all cases, similar to the flammable mass. For all cases, increasing the hydrogen storage pressure increases the available energy peak.

The energy available within the flammable range for a natural gas/methane release is smaller than for hydrogen release in all cases, and in particular for the restricted release cases (Cases 1 and 2) as the energy per unit mass is much smaller for natural gas. Restricting the outflow from the storage system (Case 2) minimizes the flammable energy peak compared with an unrestricted release (Case 3), but results in the flammable mixture being present over a longer duration.

5.2.3. Combustion

The combustion simulations provide the data required to evaluate the consequences of the release in terms of generated overpressures and fireball sizes. It must be emphasized that the information about the amount of initial flammable mixture (and therefore the initial amount

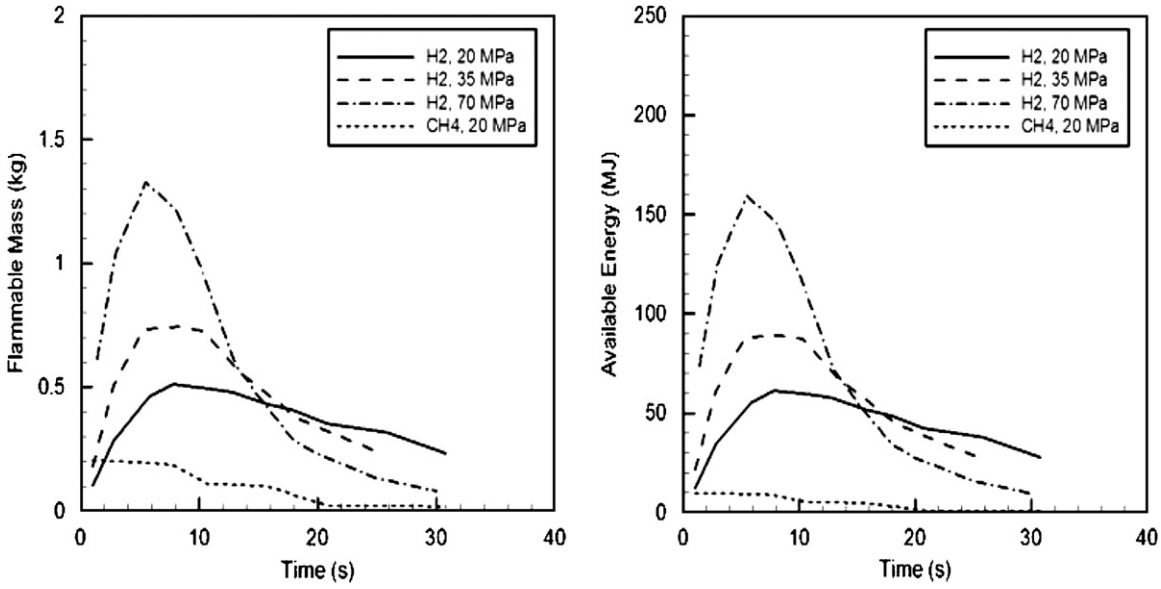

Fig. 8. Flammable mass history (left) and available energy history (right) for Case 1. (Urban environment).

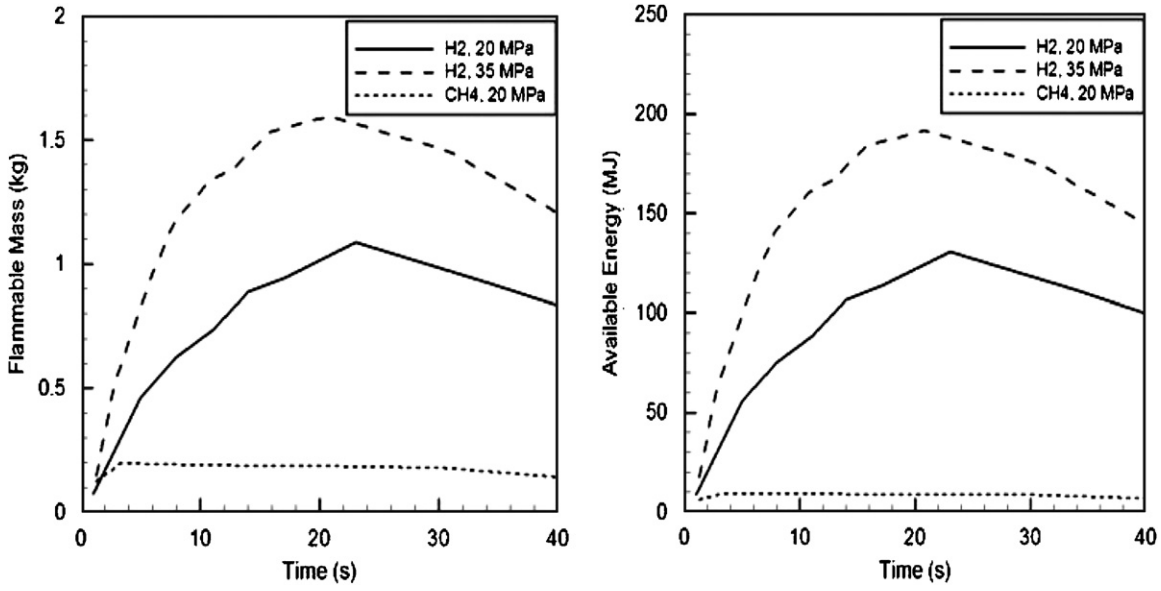

Fig. 9. Flammable mass history (left) and available energy history (right) for Case 2. (Urban environment).

of available chemical energy) must be complemented by additional information in order to have a more precise initial estimate of the potential damage that an explosion can produce. Different initial distribution of hydrogen concentration within a cloud can generate significantly different level of overpressure given the same amount of flammable mixture and the same initial geometrical configuration. In this context, the distribution of concentration ranges within the hydrogen mixture is provided in Table 5. The table shows that although the hydrogen flammability range is wide, a significant proportion of the flammable mixture is in the range of 4–10%, which is the least reactive region. Another significant proportion is in the range 10-14%, which still has relatively low reactivity, especially for a relatively unconfined configuration with a very small blockage ratio such as a 14 m wide street canyon with vehicles. It is well known that the effect of confinement and obstacles is to increase the flame speed and the generated overpressure, as demonstrated in many experimental works such as the investigation of Moen, Lee, Hjertager, Fuhre, and Eckhoff (1982). In case of unconfined and unobstructed configurations, the flame propagates with smaller velocities than in a confined and obstructed geometry. It has been shown experimentally that in an unconfined 10 m diameter cloud of stoichiometric (~29.5%) hydrogen air mixture, the flame propagates as a

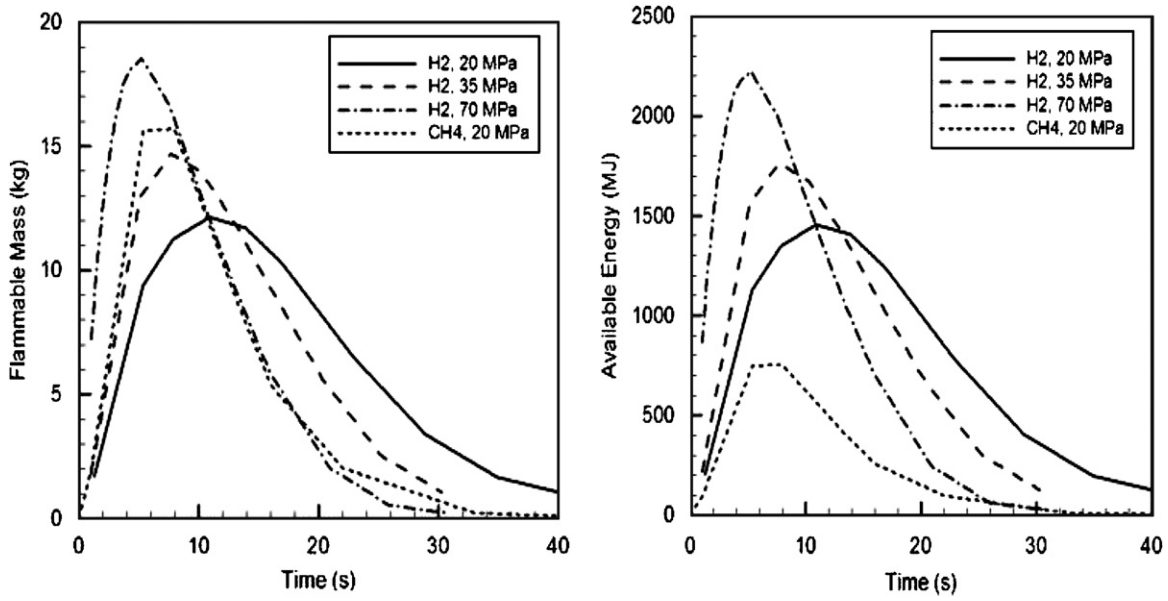

Fig. 10. Flammable mass history (left) and Available energy history (right) for Case 3. (Urban environment) (Note: The vertical scale is larger than Figs. 8 and 9).

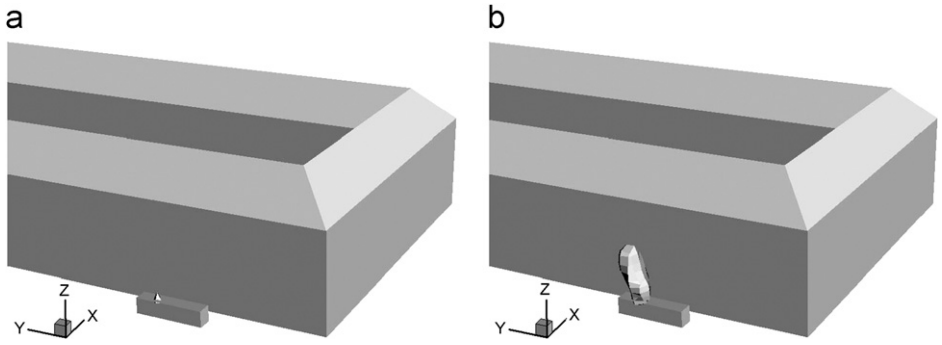

Fig. 11. Predicted LFL cloud for Case 1, where (a) CH_4, 20 MPa at 1.0 s, (b) H_2, 35 MPa at time 8.3 s.

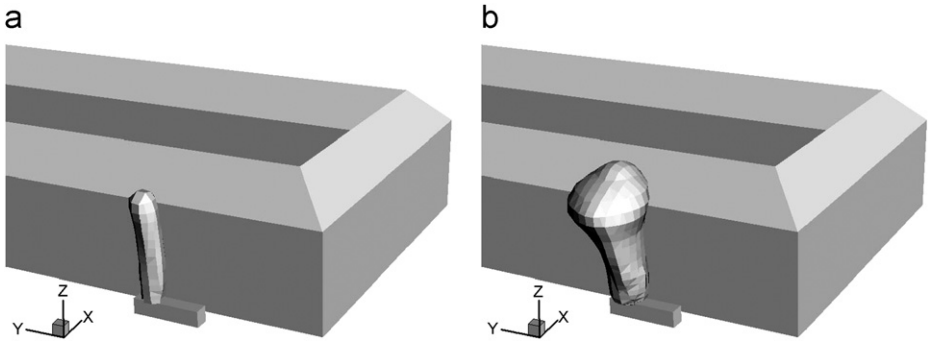

Fig. 12. Predicted LFL cloud for Case 3, where (a) CH_4, 20 MPa at 7.9 s, (b) H_2, 35 MPa at time 7.7 s.

Table 4
Lower heat of combustion

Fuel	Lower heat of combustion (MJ kg^{-1})
Hydrogen	120
Natural gas	48

slow deflagration (Becker & Ebert, 1985; Schneider & Pförtner, 1983), generating overpressures smaller than 10 kPa.

The ignition position was located above the bus roof, within 1 m distance of the release source(s). This chosen ignition pint is well within the flammable cloud and at this

Table 5
Amount of hydrogen mass (kg) in the initial flammable mixture, according to volumetric concentration (urban environment)

Case	Pressure (MPa)	Ignition time (s)	Conc. range 4–75% (kg)	Conc. range 4–10% (kg) (%)	Conc. range 10–14% (kg) (%)
1	20	7.8	0.512	0.367 (71.5)	0.076 (14.8)
	35	8.3	0.743	0.551 (74.1)	0.119 (16)
	70	5.5	1.327	0.935 (70.4)	0.238 (17.9)
2	20	23.0	1.088	0.908 (83.4)	0.111 (10.2)
	35	20.8	1.596	1.245 (78.0)	0.204 (12.7)
3	20	10.9	12.145	6.474 (53.3)	2.645 (21.7)
	35	7.7	14.691	6.454 (43.9)	3.417 (23.2)
	70	5.2	18.526	7.360 (39.7)	3.861 (20.8)

Note: In brackets, the same amount of hydrogen at that concentration is expressed as percentage of the total amount of hydrogen in the flammable cloud.

height electrical installations such as streetlights might cause accidental ignition. The ignition time has been selected at the time of the maximum mass of flammable mixture in the explosive cloud. This condition occurs between 5 and 23 s after the start of the release depending on the particular case, as shown in Figs. 8–10 and in Table 5. One of the worst case scenarios has been modelled as there are many possible outcomes for the release cases modelled depending on the bus, the storage system and pressure, etc., and if applicable the fire. It was considered to be more important to understand the outer envelope of possible releases, than to model one of the many other but less severe scenarios that could be foreseen. Assuming ignition at the time when the maximum flammable mass occurs is not overly extreme. Anecdotal reports by various research and testing organizations indicate that, fires that cause temperature triggered PRDs to open, may not immediately ignite the vented gas. The fire that triggers the thermally activated PRD may not be in a position that causes the vented gas to ignite, since the exit from the vent may not be situated in the fire. Hence delayed ignition as the flammable cloud builds and expands to an ignition source is an acceptable assumption.

In the simulations, the explosions propagate as a deflagration and that is consistent with the amount of flammable mixture, the mixture concentration distribution and the relatively low level of confinement in the street canyon.

The results of the combustion modelling were interpreted in terms of overpressure effects and direct flame impingement. For the purposes of this study a simplistic interpretation of the direct blast overpressure effects was satisfactory, and detailed results in the form of direct blast impulses and indirect blast effects were not derived. In order to analyse the results, three key overpressure thresholds have been identified, according to a review of common consequence assessment criteria:

- 2 kPa: threshold of window breakage (10% broken windows).
- 21 kPa: threshold of eardrum rupture and moderate building damage.
- 35 kPa: severe building damage.

Due to the low heat transfer from hydrogen flames by radiation and the relatively short combustion time, radiation is not taken into account in this investigation. It is a well-known fact that methane flames give off more heat by radiation than hydrogen flames. Direct flame impingement in terms of fireball size has been used as a measure of heat effects.

The combustion results are summarized in Table 6. In this table the overpressures are indicated as contours, e.g. the "distance to 2 kPa overpressure" is the distance from the ignition point at which the overpressure drops below 2 kPa. Similar definition holds for distances to 21 and 35 kPa. The pressure contours have been identified using iso-surface plots similar to those shown in Fig. 13.

As expected from the dispersion results, Case 3 is the worst case in terms of combustion, while negligible differences were apparent between Cases 1 and 2 in terms of overpressure and size of the fireball. For all cases, the larger the storage pressure, the larger is the generated overpressure. For the hydrogen cases, the predicted fireball size does not increase significantly as the storage pressure increases. The predicted effects of the natural gas release are negligible for Cases 1 and 2. For Case 3 the predicted effects of the natural gas release were less severe than from the comparable hydrogen release at the same storage pressure, as would be expected with only 50% of the flammable energy of the hydrogen release. However, in terms of predicted far-field overpressure effects there is relatively little difference. As expected, the predicted size of the fireball was usually found to be larger than the flammable cloud at the time of ignition. Because of the convective field generated by the explosion, the edges of the flammable cloud are pushed further away from the ignition point by the expanding combustion products. If ignition occurs in Case 3, the effects could be expected to be similar to the 1983 Stockholm accident (Venetsanos et al., 2003). Although the amount of flammable gas was lower in the Stockholm accident than in Case 3, in the Stockholm accident there were elements that increased the combustion regime such as the likely location of the ignition point between the truck and the racks of gas cylinders. The presence of the obstacles such as the cylinder racks on the propagation path of the flame must have

Table 6
Combustion results (urban environment)

Scenario				Effect				
Case	Fuel	Pressure (MPa)	Energy (MJ)	Fireball		Overpressure		
				Average diameter at 2.0 m above ground (m)	Maximum diameter at any height above ground (m)	Distance to 2 kPa overpressure (m)	Distance to 21 kPa overpressure (m)	Distance to 35 kPa overpressure (m)
1	H_2	20	62	S	S	S	S	S
		35	89	4.3	7.5	L	L	L
		70	159	4.9	8.5	5	L	L
	NG	20	10	S	S	S	S	S
2	H_2	20	131	4.3	7.5	L	L	L
		35	192	4.5	7.7	5	L	L
		70	NM	NM	NM	NM	NM	NM
	NG	20	10	S	S	S	S	S
3	H_2	20	1460	12.7[a]	18.8	75	7	3
		35	1760	10.5[a]	15	91	8	3
		70	2220	16.0[a]	21.5	100	9	5
	NG	20	754	11.0[a]	15	65	L	L

S: Small flammable mass. Calculations were not performed, as the overpressures and fireball size were not expected to be significant.
L: Calculations were performed, but the overpressures were lower than the threshold.
NM: Not modelled.
[a]Based on the y axis only, as the building hindered expansion in the x direction.

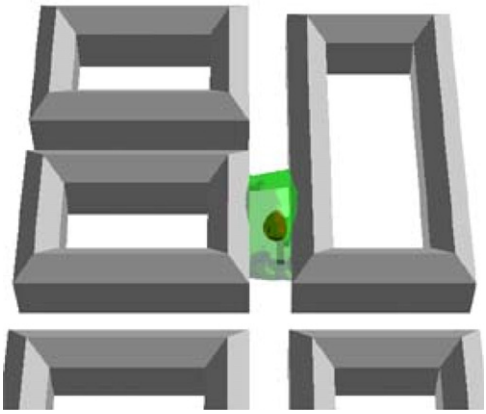

Fig. 13. Iso-surface of temperature (700 k) in red colour and iso-surface of overpressure (20 mbar) in green colour for Case 3, 70 MPa, hydrogen.

increased the turbulence–combustion interaction which is a powerful feedback mechanism for flame acceleration. For Case 3, 70 MPa hydrogen, changes in the position of the ignition point and the effects on the combustion process were investigated. Positions 1, 2 and 3 are located near the bus roof at about 3 m above the ground, position 4 is 12 m above the ground and position 5 is 20 m above the ground as shown in Table 7. The largest pressure peak at ground level is generated by the explosion in position 1 as shown in Fig. 14. The explosion in position 5 produces two pressure peaks. The second peak is generated when the flame propagates across a positive hydrogen concentration gradient: the flame starts to travel at the top edge of the

Table 7
Coordinates of ignition points. All the locations are above the bus roof (urban environment)

Position no	X (m)	Y (m)	Z (m)
1	103.5	48.5	4
2	102.5	50.5	3.4
3	101	51.5	4
4	103.5	50	12.5
5	103.5	50	20

hydrogen cloud where the hydrogen concentration is relatively low and it propagates downward toward a region with higher concentration, being closer to the release source. Since there are several important parameters that affect combustion processes when considering different ignition positions, each case must investigated separately. Unless fire is the cause of the release, it is probable that more ignition sources would be encountered at a higher level as the mixture drifts sideways or disperses upwards, e.g. street lights, air-conditioning units, overhead tram/trolley bus wires, advertisement signs, etc.

Since the combustion process is sensitive to several parameters (concentration range, concentration gradients, geometrical configuration, e.g. the level of confinement or obstruction, and ignition time and position), the results in Table 6 hold only for the initial conditions and configurations that are defined in this investigation and within the stated assumptions.

6. Tunnel environment

6.1. Modelling strategy

The same bus used in the urban environment was placed centrally in one lane of a 2-lane, bi-directional tunnel. The assumed tunnel cross-section and dimensions are shown in Fig. 15. The tunnel was assumed to have a length of 212 m. The bus was assumed to be located at the tunnel's mid-point, i.e. 100 m from each exit. As a first approach, other vehicles were not taken into account. Following suggestions from tunnel operators in the UK and Sweden, stagnant air conditions were assumed in the tunnel prior to the release, representing a worse case approach.

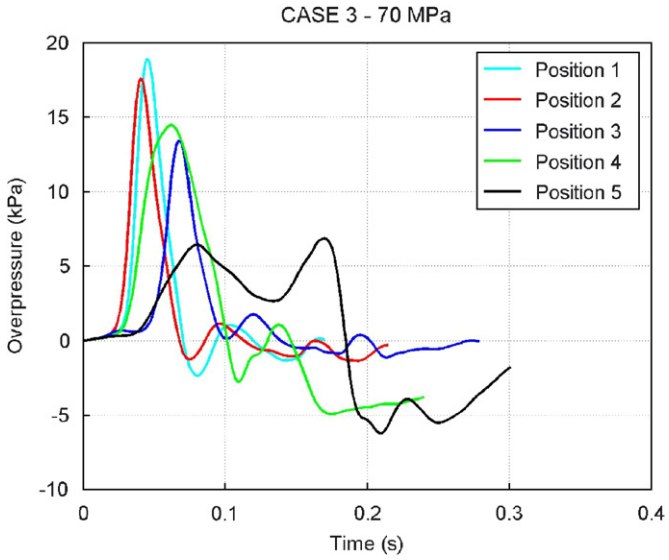

Fig. 14. Case 3, 70 MPa, hydrogen. Over-pressure history in a point that is located at ground zero at about 10 m from the bus for different positions of the ignition point. (urban environment).

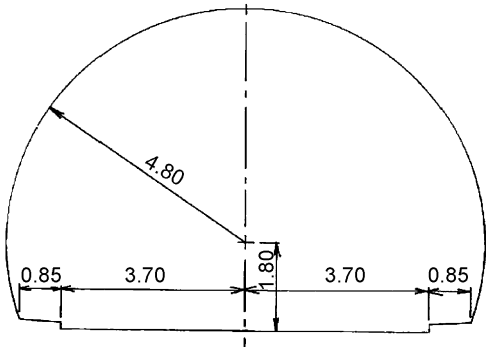

Fig. 15. Tunnel cross section.

Table 8 shows the fuel release scenarios that have been modelled. Only the two limiting scenarios Cases 1 and 3 were examined, as the consequences for Case 2 were expected to lie in between, based on the previously performed urban environment analysis.

6.1.1. Dispersion

The computational domain dimensions were $212 \times 10 \times 6.8$ m in the x (parallel to the tunnel), y and z (vertical) axis, respectively. The computational grid was Cartesian consisting of $87 \times 40 \times 34$ cells in the x, y and z directions, respectively. In the y and z directions constant step sizes of 0.25 and 0.2 m, respectively were used. The grid in the x direction was non-equidistant with minimum cell size of 0.5 m, which was kept constant around the bus. The x grid size expanded towards the tunnel exits, with a maximum x grid size of 10 m close to these exits.

Boundary conditions were as follows. Standard wall functions for velocity and turbulent kinetic energy were used on solid surfaces. Dirichlet (given value) plus Neumann (zero gradient) boundary conditions were used for the source(s). Neumann boundary conditions were used at the tunnel exits.

6.1.2. Combustion

The computational domain for the combustion calculations has the dimensions of 312 m in the longitudinal direction of the tunnel, 107 m in the transverse direction of the tunnel and 50 m vertically. The last two figures refer to the region outside the tunnel. Inside the tunnel, the resolution of the tetrahedral grid varies from a minimum distance of $\Delta x \approx 0.15$ m in the vicinity of the bus, to a grid distance of $\Delta x \approx 0.75$ m at the exit of the tunnel and to a grid distance of $\Delta x \approx 4$ m outside the tunnel. In the initial grid, the total number of computational nodes and cells are, respectively, about 92,000 and 461,000. The simulation

Table 8
Modelled fuel release scenarios (tunnel environment)

Fuel/pressure (MPa)	Case 1		Case 3	
	Dispersion model	Combustion model	Dispersion model	Combustion model
Hydrogen				
20	*Y*	*Y*	*Y*	*Y*
35	*Y*	*Y*	*Y*	*Y*[b]
70	*Y*	*Y*	–	–
Natural gas				
20	*Y*	[a]	*Y*	*Y*

[a] Effects of changing the position of the ignition point were investigated.
[b] Flammable mass too small to permit accurate combustion modelling.

employed a dynamically adaptive grid. As refinement criterion, the difference in temperature has been selected. The mesh has been refined to a grid resolution of $\Delta x \approx 0.11$ m. Due to the adaptive meshing the number of computational nodes (cells) increases during the calculations from the initial 92,000 (461,000) to some hundred thousands (few millions) depending on the case.

6.2. Results and discussion

6.2.1. Dispersion

The flammable mass of hydrogen at a given time after the start of the release is shown in Figs. 16 and 17 (left hand side) for Cases 1 and 3, respectively. Comparison is made to the corresponding figures for the urban environment (Figs. 8 and 10) and it is observed that similar to the urban environment, Case 3 (rapid release of all fuel) leads to a larger flammable mass, and Case 1 (release of fuel from only one cylinder through one outlet) to the lowest.

For the tunnel scenarios the level and shape of the predicted flammable mass history curves are different from the corresponding urban environment cases. The levels are generally much higher. The peak values occur later and decrease at a lower rate resulting in longer residence times. For hydrogen Case 1 at 35 MPa, the predicted peak hydrogen flammable mass is approximately 4 times higher in the tunnel than in the urban environment (3 kg at 30 s compared to 0.75 kg at 8 s). For hydrogen Case 3 at 35 MPa, the corresponding values are 32 and 15 kg observed at 30 and 8 s, respectively. The higher flammable mass levels and residence times observed in the tunnel can be attributed to the high level of confinement and to the assumed initially stagnant tunnel ventilation conditions.

In the urban environment analysis, the effect of increasing the storage pressure was to produce higher flammable mass peaks. The same effect can be observed in the tunnel environment, but is seen to be less important, especially for Case 3.

For methane, similar to the urban environment, the predicted flammable mass is much lower compared to hydrogen for Case 1. For Case 3, the predicted methane flammable mass is much higher than hydrogen. The same tendency for increased methane flammable mass for Case 3 was observed in the urban environment, where comparable values between hydrogen and methane were found. The behaviour in Case 1 can be attributed to the wider flammability range of hydrogen (0.04–0.75 by vol. concentration) compared to methane (0.053–0.15) and to its higher tendency to expand and occupy larger volumes than methane leading to higher concentrations. The behaviour for Case 3 can be attributed to the higher mass flow rate of methane and to the less intense turbulent mixing. The last is a result of the lower sonic velocities at the jet exit and of the lower buoyancy of methane compared to hydrogen. It can be concluded that the narrower methane flammability range and its lower expansion tendency compared to hydrogen do not guarantee flammable masses lower than for hydrogen, since factors such as the release mass flow rate and the turbulent mixing also need to be accounted for.

As with the urban environment cases, the energy present at a given time after the start of the release was estimated by converting the flammable mass data to energy by multiplying the mass of fuel by the lower heat of combustion per unit weight. The resulting energy time histories curves are shown at the right hand side of Figs. 16 and 17 (note the different vertical scale in Fig. 17). In Case 1, similar to the urban environment, the energy available for the methane release is much less than the hydrogen releases. However, in Case 3 the energy available for the methane release is greater than for the hydrogen releases, in contrast to the urban environment.

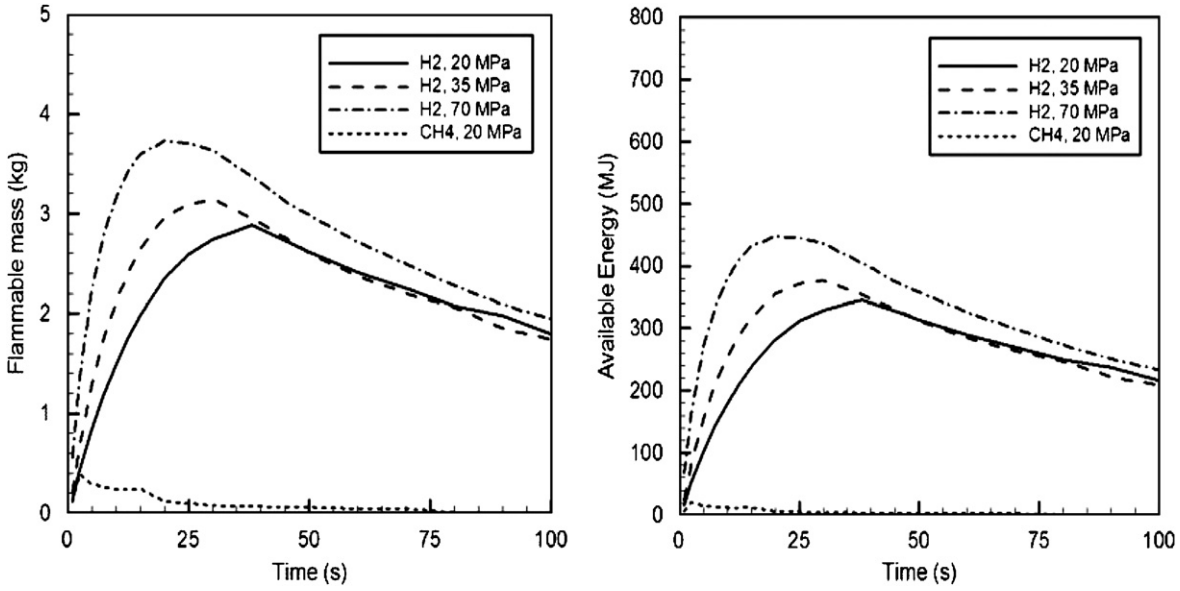

Fig. 16. Flammable mass history (left) and available energy history (right) for Case 1. (Tunnel environment).

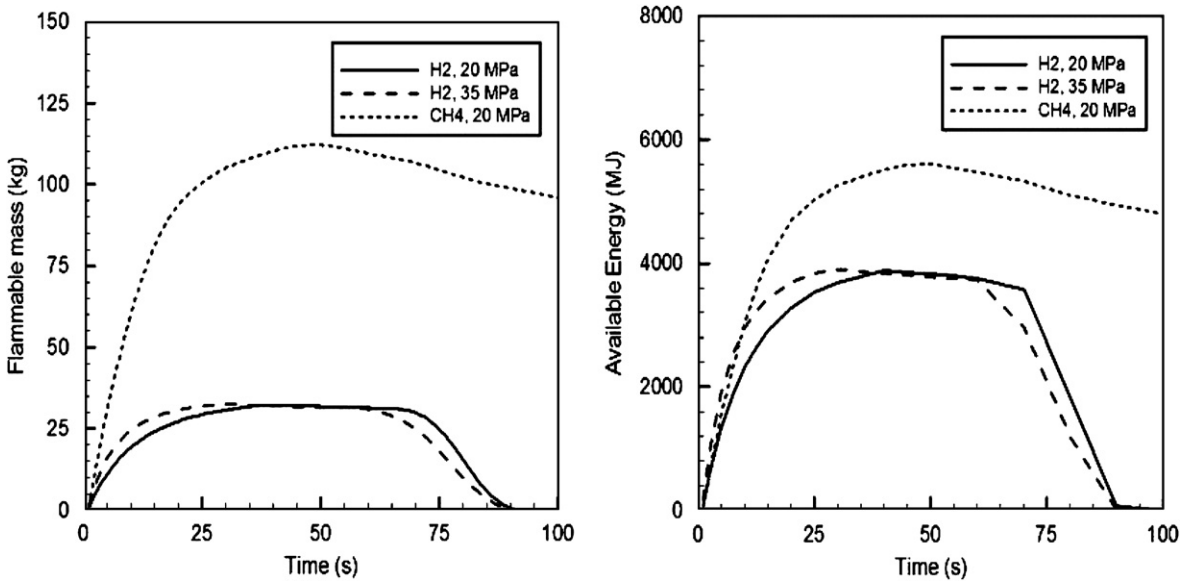

Fig. 17. Flammable mass history (left) and available energy history (right) for Case 3. (Tunnel environment) Note: The vertical scale is larger than in Fig. 16.

Table 9
Size of flammable cloud at time of ignition (tunnel environment)

Fuel	Case	Pressure (MPa)	Time after start of release (s)	Δx (m)	Volume (m^3)	Flammable fuel mass (kg)
H_2	1	20	38	53	437	2.88
		35	30	50	475	3.14
		70	20	51	519	3.73
	3	20	40	130	2358	32.38
		35	30	113	2180	32.53
NG	1	20	5	8	6	0.29
	3	20	40	69	1756	110.25

Note: Δx is distance along the tunnel length.

Figs. 16 and 17 were used to determine the time at which combustion calculations would be initiated. Similar to Venetsanos et al. (2003) and to the urban environment, the predicted flow and dispersion field, at the time of the maximum flammable fuel mass were used as initial conditions for the subsequent combustion calculations.

Table 9 shows for each case the assumed time of ignition and the corresponding "initial" size of flammable cloud. Fig. 18 shows the corresponding shapes of the predicted LFL clouds for Case 3. The LFL clouds were constructed as LFL concentration iso-surfaces. Fig. 19 shows the corresponding shapes of the predicted LFL clouds for Case 1.

It can be observed that for both Cases 1 and 3 the shapes of the hydrogen LFL clouds are similar, while the shape of the natural gas cloud is significantly different. For Case 3, at the times considered hydrogen has reached the tunnel ceiling and has moved a long distance along the ceiling away from the bus, while methane has also reached the ceiling but in contrast to hydrogen extends much further transversely and extends much less longitudinally. Table 9

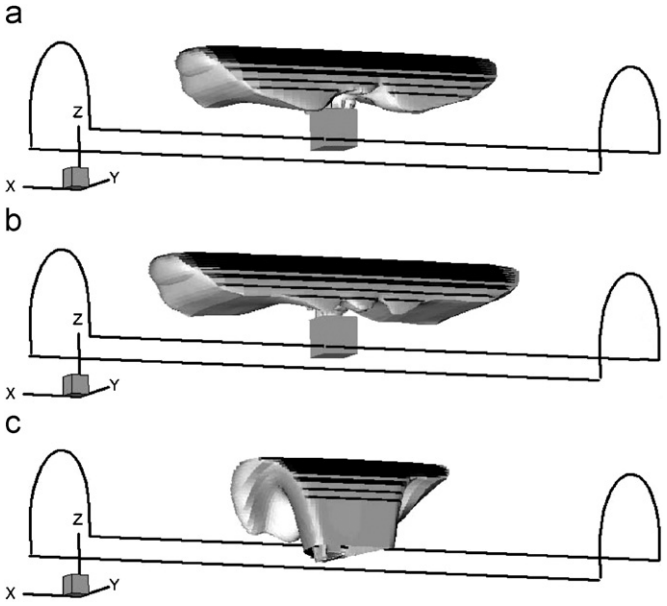

Fig. 18. Case 3: Predicted LFL cloud for (a) H_2, 35 MPa at time 30 s, (b) H_2, 20 MPa at time 40 s, (c) CH_4, 20 MPa at 40 s.

shows that for hydrogen at 20 MPa, the cloud has travelled approximately twice the distance travelled by the methane cloud, and is occupying a volume 1.34 times larger than that of methane. For Case 1 on the other hand, based on Table 9, the corresponding distance and volume ratios are much higher, namely 6.6 and 73.

6.2.2. Combustion

As already mentioned, the predicted flow and dispersion field, at the time of the maximum flammable fuel mass were used as initial conditions for the subsequent combustion calculations. Table 10 shows for each case the initial amount of hydrogen (in kg) within different flammable concentration ranges (on a volumetric basis). The figure in brackets is the amount of hydrogen at a certain concentration expressed as a percentage of the total amount of flammable hydrogen. The time after the release at which these conditions correspond is also stated. It is important to emphasize that the largest fraction of flammable hydrogen occurs in the least reactive concentration range for Case 1 (between 4% and 10%).

The potential effects after ignition were evaluated in terms of generated overpressures and fireball sizes. The ignition point was assumed located at $x = 110$ m, close to the release source, inside the tunnel, on the top of the bus roof. The two tunnel exits are located at $x = 0$ and 212 m.

Measurement points are located at regular points along the length of the tunnel. Overpressure histories at points on line 3, that is the line along one of the carriageway edges, are shown in Figs. 20–23.

The figures for Case 1 at 20 and 70 MPa are similar to Case 1 at 35 MPa. Therefore only the results for Case 1 at 35 MPa are shown herein. Positive x in the figures is for the distances from the ignition point that the blast wave travels towards the exit at $x = 212$ m, while negative x are for the blast wave that propagates towards the exit at $x = 0$ m. It can generally be observed that the blast wave maintains its strength for a long distance inside the tunnel, while in the urban environment scenarios, the blast wave decays with increasing distance from the ignition point. This difference is attributed to the higher confinement in the tunnel.

These figures also show that the overpressures for Case 3 are significantly larger (more than one order of magnitude) than in Case 1, meaning that Case 3 is potentially a far more dangerous scenario than Case 1, as expected given the larger amount of flammable gas and confinement in Case 3.

In these figures the pressure profiles for points at a distance larger than 106 m are the pressure history for points outside the tunnel. The resolution of the computational mesh outside the tunnel is coarse compared to the resolution inside the tunnel therefore the physical drop in the pressure outside the tunnel due to the physical expansion is partly enhanced by numerical effects.

Predicted peak overpressures for each case as well as calculated fireball size (in terms of length along the tunnel) are summarized in Table 11 along with the corresponding input parameters.

For Case 1, it can be observed that the peak overpressures associated with the hydrogen releases are similar and independent of the initial tank pressure, which is consistent with the available flammable energy. The overpressures are sufficient to cause glass breakage of house windows.

The extent of the hydrogen fireball for Case 1 decreases with increasing original storage pressure, which is consistent with the figures for the extent of the flammable cloud at the time of ignition. This may be due to the dynamics of the vertical release against the tunnel ceiling.

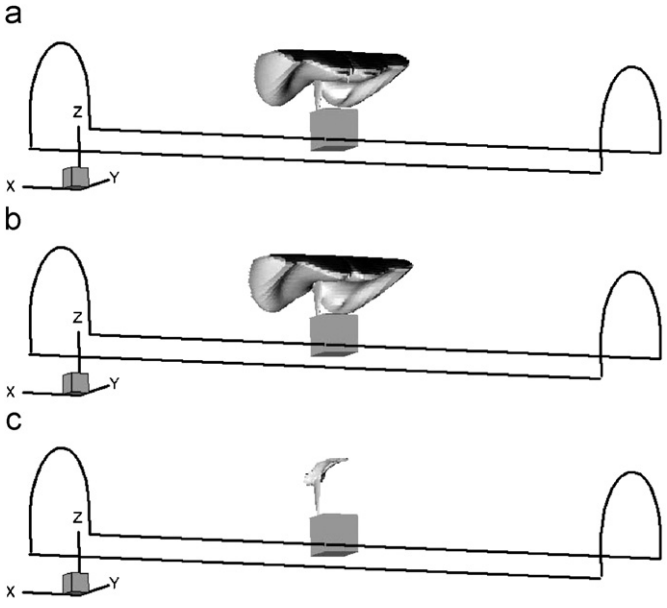

Fig. 19. Case 1: Predicted LFL cloud for (a) H_2, 35 MPa at time 30 s, (b) H_2, 20 MPa at time 38 s, (c) CH_4, 20 MPa at 5.0 s.

Table 10
Amount of hydrogen mass (kg) in the initial flammable mixture, according to volumetric concentration range (tunnel environment)

Case	Pressure (MPa)	Time after start of release (s)	Conc. range 4–75% (kg)	Conc. range 4–10% (kg) (%)	Conc. range 10–14% (kg) (%)	Conc. range 14–20% (kg) (%)	Conc. range 20–30% (kg) (%)
1	20	38	2.88	2.27 (78.8)	0.49 (17)	0.083 (2.9)	0.019 (0.6)
	35	30	3.14	2.67 (85)	0.37 (11.8)	0.069 (2.2)	0.016 (0.5)
	70	20	3.73	2.91 (78)	0.73 (19.6)	0.054 (1.4)	0.017 (0.4)
3	20	40	32.38	4.34 (13.4)	4.39 (13.6)	10.85 (33.5)	12.73 (39.3)
	35	30	32.53	3.63 (11.1)	3.62 (11.1)	8.71 (26.8)	16.35 (50.26)

Note: The amount of hydrogen in a particular concentration range is expressed as percentage of the total amount of flammable hydrogen in brackets.

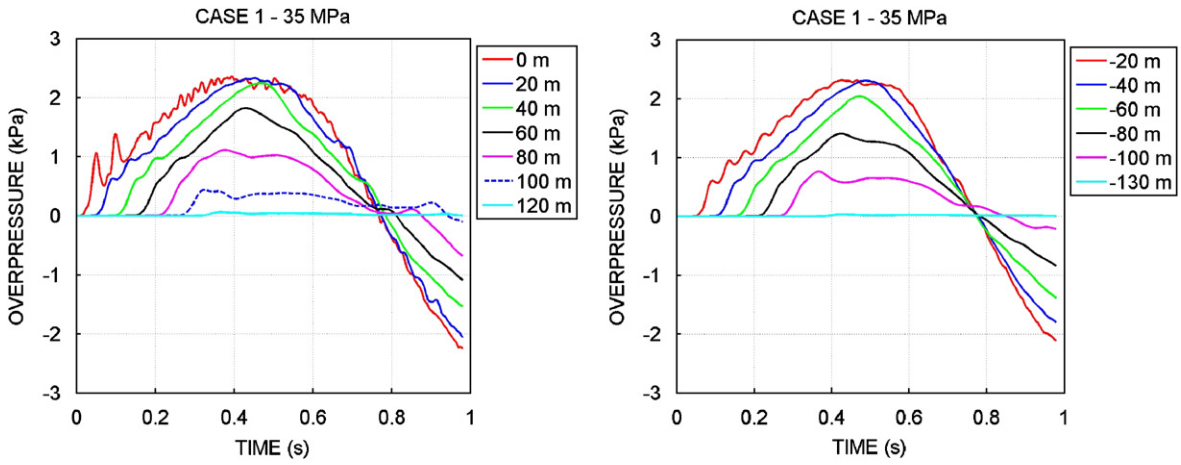

Fig. 20. Case 1, 35 MPa, hydrogen. Pressure history in points that are placed at a distance from the ignition point according to the legend. (tunnel environment).

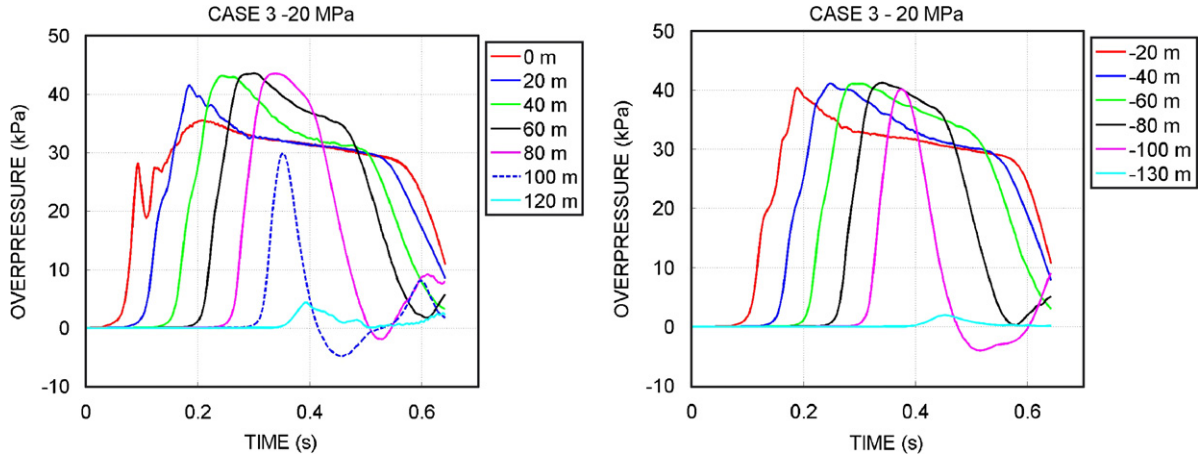

Fig. 21. Case 3, 20 MPa, hydrogen. Pressure history in points that are placed at a distance from the ignition point according to the legend. (tunnel environment).

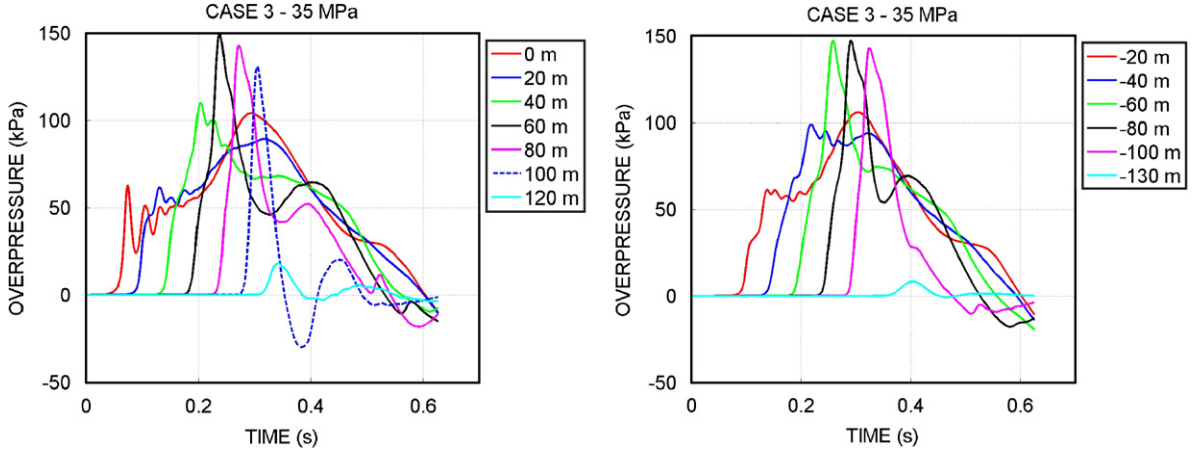

Fig. 22. Case 3, 35 MPa, hydrogen. Pressure history in points that are placed at a distance from the ignition point according to the legend. (tunnel environment).

For natural gas Case 1, the flammable mass is so low (less than 0.5 kg and in average concentrations far from stoichiometric) that negligible overpressures could be expected.

For Case 3, although the energy is identical for both hydrogen cases, the extent of the fireball in the 35 MPa release is significantly greater than for the 20 MPa release. For the later case the flame reaches the exits of the tunnel,

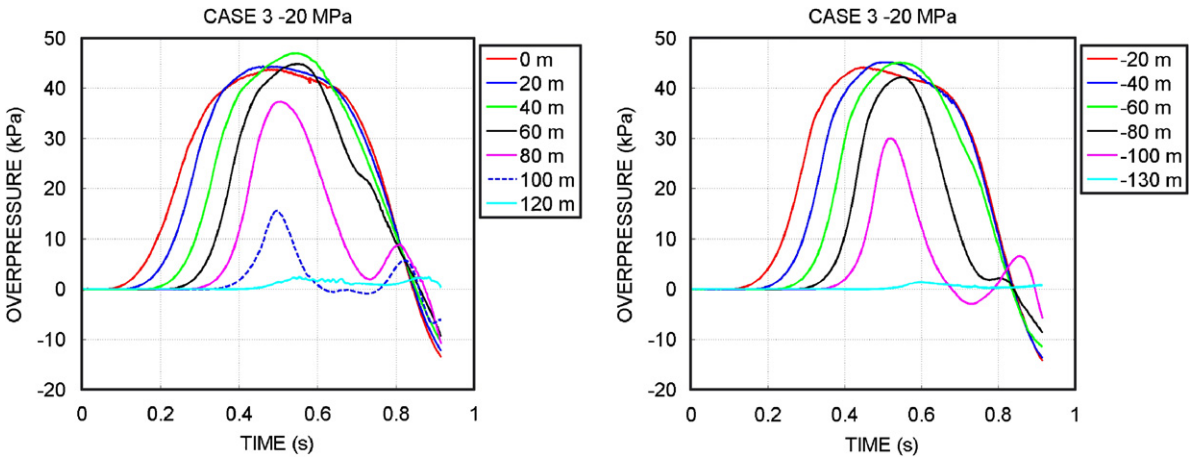

Fig. 23. Case 3, 20 MPa, methane. Pressure history in points that are placed at a distance from the ignition point according to the legend. (tunnel environment).

Table 11
Combustion results (tunnel environment)

Scenario				Effect	
Case	Fuel	Pressure (MPa)	Energy (MJ)	Fireball Length along the tunnel (m)	Overpressure Peak overpressure (kPa)
1	H_2	20	346	62	2.3
		35	377	58	2.3
		70	448	47	2.3
	NG	20	19	S	S
3	H_2	20	3890	220[a]	42.5
		35	3900	285[a]	150
		70	NM	NM	NM
	NG	20	5380	198	45

Notes: S: Small flammable mass. Calculations were not performed, as the overpressures and fireball size were not expected to be significant. NM: Not modelled. Typical overpressure effects (based on various scientific sources): 2 kPa: Threshold of window breakage. 21 kPa: Threshold of eardrum rupture and moderate building damage. 35 kPa: Severe building damage, i.e. unusable.

[a]The flame extends beyond the limits of the tunnel (tunnel length = 212 m).

while for the former it travels beyond the end. Similarly the overpressure for the 35 MPa hydrogen release is much greater than for the 20 MPa release. The significant differences for Case 3 in the effects between the 20 and 35 MPa releases despite almost identical energy, is attributed to the different distribution of flammable hydrogen mass within the flammable concentration range. As shown in Table 10, in the case at 35 MPa, more than half of the flammable mass is in the stoichiometric concentration range between 20% and 30% hydrogen, which is very reactive.

Similar to Case 1, flame size in Case 3 is larger than the size of the initial flammable cloud (see Table 9 for comparison). For Case 3, 35 MPa, the flame size is about 2.5 times the size of the initial flammable cloud.

As regards the natural gas/Case 3 release, although it has higher peak energy than either hydrogen case, the overpressure is only slightly higher than the 20 MPa hydrogen release.

The overpressures predicted for Case 3 both for hydrogen and natural gas are sufficient to cause structural damage to many forms of construction.

Figs. 24–26 show predicted concentration, temperature and pressure iso-surfaces at various times for hydrogen Case 3 at 20 MPa. Fig. 24 illustrates a front view of the hydrogen cloud in blue colour and the propagation of the flame front in red colour shortly after ignition. The ignition point is placed on the top of the bus close to the release. Figs. 25 and 26 show the pressure iso-surface in yellow colour in addition to the hydrogen concentration and the flame front at 100 and 290 ms, respectively. Those times are calculated from the ignition time (ignition time = 0 ms). The pressure iso-surfaces in the figures do not identify the maximum pressure but simply show the propagation of the blast wave along the tunnel.

The above cases assume an ignition point on top of the bus. When an alternative ignition point was tested for Case 3, 20 MPa hydrogen, approximately 50 m from the bus on

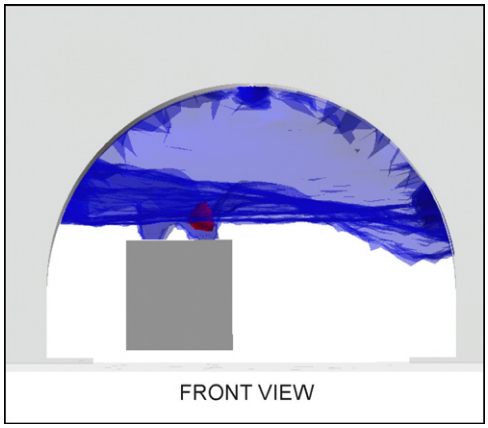

Fig. 24. Case 3, 20 MPa, hydrogen cloud. Initial hydrogen distribution: concentration iso-surface in blue colour (7%). Temperature iso-surface in red colour (700 K). Time: 10 ms.

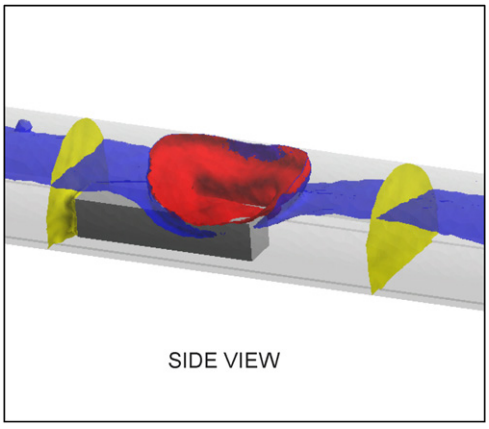

Fig. 25. Case 3, 20 MPa, hydrogen. Concentration iso-surface in blue colour (7%). Temperature iso-surface in red colour (1500 K). Overpressure iso-surface in yellow colour (21 kPa). Time: 100 ms.

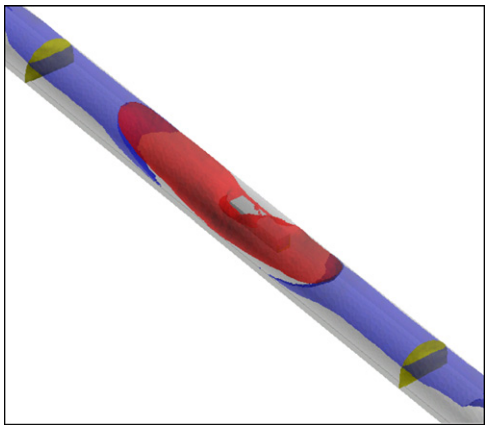

Fig. 26. Case 3, 20 MPa, hydrogen. Concentration iso-surface in blue colour (7%). Temperature iso-surface in red colour (1500 K). Overpressure iso-surface in yellow (21 kPa) Time: 290 ms.

the tunnel wall (close to the edge of the flammable cloud), substantially higher peak overpressures were calculated in excess of 200 kPa, as shown in Fig. 27. This difference in pressure can be explained by a different combustion regime: with the new ignition position, the flame front travels as a much faster deflagration compared to the case with the first ignition point on top of the bus. Two combustion regimes occurred modifying the position of the ignition because the hydrogen cloud is highly non-uniform in terms of H_2 concentration and turbulence, with the larger concentration and turbulence in the regions close to the release source. This gives a further confirmation that the position of the ignition point can affect significantly the combustion process as already shown in the urban environment.

7. Conclusions

CFD analyses were undertaken for hydrogen and natural gas releases from compressed gaseous systems on commercial vehicles in urban and tunnel environments. Hydrogen releases from storage systems with nominal working pressures of 20, 35 and 70 MPa, and a comparative natural gas release (20 MPa) were considered.

The scenarios investigated are based on the assumptions that either fire causes a release via a thermally activated PRD and that the released gas vents without immediately igniting, or that a PRD fails. Three different release strategies were considered: Case 1 with the content of only one cylinder (hydrogen—5 kg or methane—21 kg) released through one vertical outlet above the roof, Case 2 with the gas from all cylinders released into the atmosphere through the same vertical outlet as in Case 1 and Case 3 with the gas from the entire storage system (eight cylinders containing hydrogen—40 kg-or natural gas—168 kg) released through four vertical outlets above the roof. Late ignition was assumed at the time of occurrence of the maximum flammable mass present in the atmosphere. The main conclusions from the cases investigated are given below.

Regarding the release mass flow rate, the higher the tank pressure, the larger is the flow rate. The higher density of methane and the larger initial amount of methane in the tank cause a larger and longer lasting mass flow rate for methane than for hydrogen.

For the urban environment, regarding the released flammable mass, for a given release strategy, the effect of a higher storage pressure is to produce higher flammable fuel mass peaks occurring at times closer to the start of the release. The predicted hydrogen flammable masses are comparable to methane for Case 3, rapid release rate, but are significantly larger in the other two scenarios despite the mass flow rate being higher for methane in all cases. In terms of the available energy, the higher the tank pressure, the larger is the energy. Restricting the outflow from the storage system (Case 2) minimizes the flammable energy peak compared with an unrestricted release (Case 3), but results in the flammable mixture being present over a longer duration. The energy available within the flammable range for a natural gas (methane) release is smaller than for hydrogen release in all cases, and in particular for the

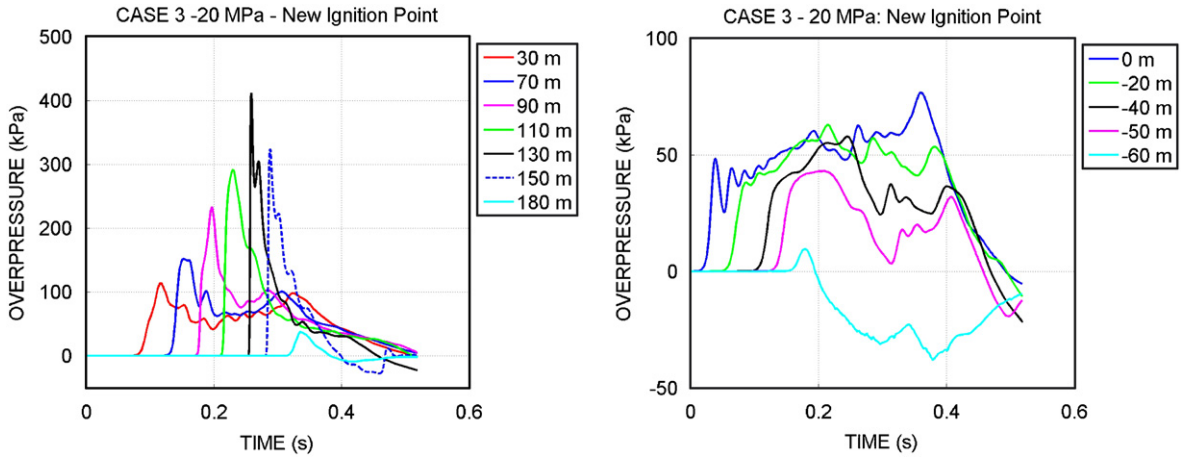

Fig. 27. Case 3, 20 MPa, hydrogen. New ignition point. Pressure history in points that are placed at a distance from the ignition point according to the legend. (Tunnel environment).

restricted release cases (Cases 1 and 2) as the energy per unit mass is much smaller for natural gas. As expected from the dispersion results, the predicted overpressures generated by combustion increase with increasing hydrogen storage pressure. Case 3 is the worst case in terms of overpressure and size of the fireball during combustion, while negligible differences were recorded between Cases 1 and 2. If ignition occurs in Case 3, the effects could be expected to be similar to the 1983 Stockholm accident. In the cases where the hydrogen release is restricted, by venting through a single PRD (Cases 1 and 2), the effects are relatively minor and localized close to the area of the flammable cloud. Even in the relatively confined environment considered, the effects on the combustion regime are closer to what would be expected in a more open environment, i.e. a slow deflagration should be expected. It was also shown that the ignition position affects the level of overpressure. For one ignition position, multiple overpressure peaks were generated.

By far the most critical case investigated in any of the environments was a rapid release of the entire hydrogen or natural gas storage system within the confines of a non-ventilated tunnel (Case 3). In this case, there was minimal difference between a release from a 20 MPa natural gas system or a 20 MPa hydrogen system, however, a similar release from a 35 MPa hydrogen system was significantly more severe and particularly in terms of predicted overpressures. The significant differences in the effects between the 20 and 35 MPa releases despite almost identical energy, was attributed to the different distribution of hydrogen mass within the flammable concentration range inside the clouds formed during the releases. Mitigating measures must be developed to avoid Case 3 occurring in a tunnel. A restricted release (Case 1) in a tunnel, though substantially less severe than Case 3 by an order of magnitude in terms of energy and overpressure, and less than one third in terms of fireball extent, is still more severe than a similar release in the relatively unconfined urban environment. Based on the predicted overpressures, typical effects could be damaged vehicle windows or tunnel lighting units. A simple method of mitigating the effects could be the installation of plastic or toughened glass tunnel lighting units (that avoid fracture into shards of glass). For Case 1 in a tunnel, there is not a significant difference between hydrogen storage pressures in terms of the energy available after a release and on the effects. However, for Case 3 there is a significant increase in the effects with increasing hydrogen storage pressure. The study has also highlighted that the ignition point significantly affects the combustion regime in confined environments. The results have indicated that critical cases in tunnels may tend towards a fast deflagration or where there are turbulence generating features, e.g. multiple obstacles, there is the possibility that the combustion regime could progress to a detonation.

When comparing the urban and tunnel environments, a similar release of hydrogen has the potential to be significantly more severe in a tunnel, and the energy available in the flammable cloud is greater and remains for a longer period in tunnels.

When comparing hydrogen and natural gas releases, for the cases and environments investigated and within the limits of the assumptions, it appears that hydrogen requires different mitigation measures in order to have the same potential consequences as those of natural gas in case of an accident.

The principal conclusions to be drawn from this study, considering both tunnel and urban environments, with respect to a PRD opening strategy for hydrogen storage systems are that systems should be designed to avoid simultaneous opening of all PRD. For the potential effects of the released energy to be mitigated, either the number of PRDs opening should be limited or their vents to atmosphere should be restricted. For the latter point consideration must be given to optimizing the pressure build up/hydrogen release rate and ability of the containers to withstand fire for a particular system. In the urban environment, there is relatively little difference in terms of the maximum energy available in the flammable cloud

between one container venting through a single PRD and all containers venting through a single PRD, however, the duration over which the energy is available is much longer for the latter case. A similar trend is expected for the tunnel environment.

Finally, the work undertaken has proven CFD modelling techniques to be a useful tool for investigating the release of hydrogen in real world situations. It also underlines the importance and benefits of performing safety studies for hydrogen applications, in order to be able to understand, and therefore, minimize and control the consequences of accidental hydrogen releases to within acceptable levels.

As a result of the work undertaken, the following recommendations are made for further research:

- The effect of the fuel concentration range within a flammable cloud on the combustion regime and therefore on overpressures. Future studies must also consider the effect of different ignition times and positions in the same accident scenario.
- The effects of wind on the dispersion and combustion of hydrogen.
- Hydrogen releases in tunnels must be investigated further to gain a better understanding of the release and ignition conditions that could result in fast deflagrations or detonations, including the effect of ventilation, different tunnel characteristics and the blockage ratio due to the presence of vehicles in the tunnel, including realistic mixes of heavy and light vehicles.
- For PRD release strategies, a detailed risk analysis is necessary before any detailed recommendations can be made. Such an analysis would have to balance the risks associated with the consequences of venting the gas from the storage system as quickly as possible and the possibility of an explosion, against restricting the energy flow from the storage system so that the explosion risk is reduced but with an increased risk of an uncontrolled release from a fire damaged tank sytem, e.g. failed overwrap or melting of a non-metallic liner. The study would also have to take into account the possibility of PRD (component) failures. A possible restriction could be made on the mass or energy flow from the system linked to a requirement to avoid premature failure of the overwrap or liner. Container assemblies containing a number of containers with perhaps a single PRD would have to be given special attention. Additional issues that could be considered are:
  - Whether PRD vents that disperse the hydrogen faster by generating turbulence rather than by venting via a straight jet, could result in the combustion regime tending towards fast deflagration or detonation.
  - Would direct ignition of the vented hydrogen resulting in a jet fire be preferable to dispersion and the associated possibility of an explosion.
  - Should the requirements be redrafted so that the containers have to withstand fire for a specified period (based on typical vehicle fires or tunnel fires) without structural failure or venting of the hydrogen, i.e. without PRDs fitted?

Acknowledgement

The authors would like to thank the European Commission for funding of this work in the framework of the EC project European Integrated Hydrogen Project—Phase 2 (EIHP-2 EC Contract no: ENK6-CT2000-00442).

References

Adams, P. (2000). Final report 01.02.98 to 30.04.00 for the European integrated hydrogen project. Volvo Technological Development Corporation, Doc. no. 06120-00-853-1.

Adams, P., et al. (2004). *Identification of the optimum on-board storage pressure for gaseous hydrogen city buses, sub-task 3.1*. European integrated hydrogen project—phase 2 ⟨http://www.eihp.org/⟩.

AL. (1976). *Encyclopedie des gaz, L'Air Liquide. Division scientifique*, Vol. VII. Amsterdam: Elsevier.

Andronopoulos, S., Bartzis, J. G., Würtz, J., & Asimakopoulos, D. (1994). Modelling the effects of obstacles on the dispersion of denser than air gases. *Journal of Hazardous Materials*, *37*, 327–352.

Baraldi, D., Heitsch, M., Eyink, J., Mohaved, M., Dorofeev, S., Kotchourko, A., et al. (2003). Application and assessment of hydrogen combustion models. *The 10th int. topical meeting on nuclear reactor thermal hydraulics* (*NURETH-10*). Seoul, Korea.

Bartzis, J. G. (1991). ADREA-HF: *A three-dimensional finite volume code for vapour cloud dispersion in complex terrain*. Report EUR 13580.

Becker, T., & Ebert, F. (1985). Vergleich zwischen experiment und theorie der explosion grober, freier Gaswolken. *Chemie Ingenieur Technik*, *57*, 42–45.

Bielert, U., Breitung, W., Kotchourko, A., Royl, P., Scholtyssek, W., Veser, A., et al. (2001). Multi-dimensional simulation of hydrogen distribution and turbulent combustion in severe accidents. *Nuclear Engineering and Design*, *209*, 165–172.

Birch, A. D., Brown, D. R., Dodson, M. G., & Swaffield, F. (1984). The structure and concentration decay of high pressure Jets of natural gas. *Combustion Science and Technology*, *36*, 249–261.

Birch, A. D., Hughes, D. J., & Swaffield, F. (1987). Velocity decay of high pressure jets. *Combustion Science and Technology*, *52*, 161–171.

Breitung, W., Dorofeev, S., Kotchourko, A., Redlinger, R., Scholtyssek, W., Bentaib, A., et al. (2005). Integral large scale experiments on hydrogen combustion for severe accident code validation—HYCOM. *Nuclear Engineering and Design*, *235*, 253–270.

Breitung, W., Necker, G., Kaup, B., & Veser, A. (2001). Numerical simulation of hydrogen in a private garage. *In Proceedings of the 4th international symposium on hydrogen power—Theoretical and engineering solutions—Hypothesis* Vol. IV, 9–14 September, Stralsund, Germany.

Ewan, B. C. R., & Moodie, K. (1986). Structure and velocity measurements in under-expanded jets. *Combustion Science and Technology*, *45*, 275–288.

FZK, (1999). Hydrogen research at Forschungszentrum Karlsruhe. In *Proceedings of the workshop on dissemination of goals, preliminary results and validation of methodology. EC-DG XII*. Brussels, March 11 ⟨www.eihp.org/eihp1/workshop⟩.

Gallego, E., García, J., Migoya, E., Crespo, A., Kotchourko, A., Yanez, J., & Beccantini, A., et al. (2005). An inter-comparison exercise on the capabilities of CFD models to predict deflagration of a large-scale H_2–Air mixture in open atmosphere. In *First international conference on hydrogen safety*, 8–10 September, Pisa, Italy.

Gallego, E., Migoya, E., Martín-Valdepeñas, J. M., Crespo, A., García, J., & Venetsanos, A. G., et al. (2007). An inter-comparison exercise on the capabilities of CFD models to predict distribution and mixing of hydrogen in a closed vessel. *International Journal of Hydrogen Energy*, in press (available online 25 May 2007).

Grasso, F., & Meola, C. (1996). Euler and Navier–stokes equations for compressible flows: Finite–volume methods. In R. Peyret (Ed.), *Handbook of computational fluid mechanics*. London: Academic Press.

Heggem, P. S. (2002). *Private communication*. Raufoss Fuel Systems AS, e-mail March 6.

Hjertager, B. H. (1982a). Simulation of transient compressible turbulent reactive flows. *Combustion Science and Technology*, *41*, 159–170.

Hjertager, B. H. (1982b). *Numerical simulation of flame and pressure development in gas explosions, SM study No 16*. Ont.: University of Waterloo Press (pp. 407–426).

Hjertager, B. H. (1989). Simulation of gas explosions. *Modelling, Identification and Control*, *10*, 227–247.

Hjertager, B. H. (1993). Computer modelling of turbulent gas explosions in complex 2D and 3D geometries. *Journal of Hazardous Materials*, *34*, 173–197.

Hjertager, B. H., & Solberg, T. (1999). A review of computational fluid dynamics (CFD) modelling of gas explosions. In V. E. Zarko, et al. (Eds.), *Prevention of hazardous fires and explosions* (pp. 77–91). Kluwer Academic Publishers.

HLG. (2003). *The high level group for hydrogen and fuel cells. Hydrogen energy and fuel cells, a vision for our future*. Final report EUR 20719 EN.

Huld, T., Peter, G., & Staedtke, H. (1996). Numerical simulation of explosion phenomena in industrial environment. *Journal of Hazardous Material*, *46*, 185–195.

ISO-IEC Guide 51. (1999). Safety aspects. *Guidelines for their inclusion in standards* (second ed.).

John, J. E. A. (1978). *Gas dynamics* (p. 394). Alyn and Bacon, Inc.

Koroll, G. W., Kumar, R. K., & Bowles, E. M. (1993). Burning velocities of Hydrogen-air mixtures. *Combustion and Flame*, *94*, 330–340.

Moen, I. O., Lee, J. H. S., Hjertager, B. H., Fuhre, K., & Eckhoff, R. K. (1982). Pressure development due to turbulent flame propagation in large-scale methane-air explosions. *Combustion and Flame*, *47*, 31–52.

Mukai, S., Suzuki, J., Mitsuishi, H., Oyakawa, K., & Watanabe, S. (2005). CFD simulation on diffusion of leaked hydrogen caused by vehicle accident in tunnels. *Proceedings of the first international conference on hydrogen safety*, 8–10 September, Pisa, Italy.

Naamansen, P., Baraldi, D., Hjertager, B. H., Solberg, T., & Cant, R. S. (2002). Solution adaptive CFD simulation of premixed flame propagation over various solid obstructions. *Journal of Loss Prevention in the Process Industries*, *15*, 189–197.

Niederbäumer, G., Sägesser, R., & Obrist, A. (2004). Simulation of gaseous explosions in tunnels as part of a risk-based design. In *Proceedings of the 11th loss prevention symposium*, June 1–3, Prague.

Nkonga, B., & Guillard, H. (1994). Godunov type method on non-structured meshes for three-dimensional moving boundary problems. *Computer Methods in Applied Mechanics in Engineering*, *113*, 183–204.

Popat, N. R., Catlin, C. A., Arntzen, B. J., Lindstedt, R. P., Hjertager, B. H., Solberg, T., et al. (1996). Investigations to improve and assess the accuracy of computational fluid dynamic based explosion models. *Journal of Hazardous Materials*, *45*, 1–25.

Rhodes, N. (2003). An overview of the European thematic network–fire in tunnels. *The QNET—CFD Network Newsletter*, *2*(2), 17–20.

Rivara, M. C., & Levin, C. (1992). A 3-D refinement algorithm suitable for adaptive and multi-grid techniques. *Communications in Applied Numerical Methods*, *8*, 281–290.

Roe, P. L. (1980). Approximate riemann solvers, parameter vectors, and difference schemes. *Journal of Computational Physics*, *43*, 357–372.

Rogers, G. & Mayhew, Y. (1992). *Engineering thermodynamics work and heat transfer* (4th ed.). Longman.

Schefer, R. W., Houf, W. G., Williams, T. C., Bourne, B., & Colton, J. (2006). Characterization of high-pressure, underexpanded hydrogen-jet flames. *International Journal of Hydrogen Energy*, in press, Available online 9 October 2006.

Schneider, H., & Pförtner, H. (1983). PNP-Sichcrheitssofortprogramm. *Prozessgasfreisetzung—Explosion in der Gasfabrik und Auswirkungen von Druckwellen auf das Containment*.

Statharas, J. C., Bartzis, J. G., Venetsanos, A. G., & Würtz, J. (1993). Prediction of ammonia releases using the ADREA-HF code. *Process Safety Progress*, *12*, 118–122.

Statharas, J. C., Venetsanos, A. G., Bartzis, J. G., Würtz, J., & Schmidtchen, U. (2000). Analysis of data from spilling experiments performed with liquid hydrogen. *Journal of Hazardous Materials*, *A77*, 57–75.

Swain, M. R., & Swain, M. N. (1992). A comparison of H_2, CH_4 and C_3H_8 fuel leakage in residential settings. *International Journal of Hydrogen Energy*, *17*, 807–815.

Troyer, C., Baraldi, D., Kranzlmueller, D., Wilkening, H., & Volkert, J. (2005). Parallel grid adaptation and dynamic load balancing for a CFD solver. In B. Martino, et al. (Eds.). *EuroPVM/MPI 2005,* Vol. 3666 (pp. 493–501). Lecture notes in computer science.

UN ECE WP29 GRPE Working Doc. 2004/3. Proposal for a new draft Regulation: Uniform provisions concerning the approval of: 1. Specific components of motor vehicles using compressed gaseous hydrogen; 2. Vehicles with regard to the installation of specific components for the use of compressed gaseous hydrogen 〈http://www.unece.org/trans/doc/2004/wp29grpe/TRANS-WP29-GRPE-2004-03e.doc〉.

US Department of Energy. (2002). *A national vision of America's transition to a hydrogen economy—To 2030 and beyond.*

Venetsanos, A. G., & Bartzis, J. G. (2007). CFD modelling of large-scale LH2 spills in open environment. *International Journal of Hydrogen Energy*, in press (available online 23 May 2007).

Venetsanos, A. G., Bartzis, J. G., Würtz, J., & Papailiou, D. D. (2000). Comparative modelling of a passive release from an L-shaped building using one, two and three-dimensional dispersion models. *International Journal of Environment and Pollution*, *14*, 324–333.

Venetsanos, A. G., Huld, T., Adams, P., & Bartzis, J. G. (2003). Source, dispersion and combustion modelling of an accidental release of hydrogen in an urban environment. *Journal of Hazardous Materials*, *A105*, 1–25.

Vlachogiannis, D., Rafailidis, S., Bartzis, J. G., Andronopoulos, S., & Venetsanos, A. G. (2002). Modelling of flow and pollution dispersion in different urban canyon geometries, water, air and soil pollution. *Focus*, *2*, 405–417.

Wilkening, H. & Baraldi, D. (2006). An innovative method of adaptive meshing for hydrogen explosion simulations with the CFD code REACFLOW. *Jahrestagung Kerntechnik-annual meeting on nuclear technology*, Aachen.

Wilkening, H., & Huld, T. (1999). An Adaptive 3D CFD solver for modelling explosions on large industrial environmental scales. *Combustion Science Technology*, *149*, 361–387.

Wilkening, H., Venetsanos, A. G., Huld, T., & Bartzis, J. G. (2000). Safety assessment of hydrogen as a fuel for vehicles by numerical simulations. *Euro-conference on new and renewable technologies for sustainable development*, 26–29 June, Madeira, Portugal.

Würtz, J., Bartzis, J. G., Venetsanos, A. G., Andronopoulos, S., Statharas, J., & Nijsing, R. (1996). A dense vapour dispersion code package for applications in the chemical and process industry. *Journal of Hazardous Materials*, *46*, 273–284.

Zalosh, R., Amy, J., Hofmeister, C., & Wang, W. (1994). *Dispersion of CNG fuel releases in naturally ventilated tunnels*. Final report, Center For Fire Safety Studies, Worcester Polytechnic Institute, Worcester MA 01609-2280, US. (p. 42).